ESCOLA SUPERIOR DE TECNOLOGIA DA SAÚDE DE LISBOA
Instituto Politécnico de Lisboa

INSTITUTO POLITÉCNICO DE LISBOA
ESCOLA SUPERIOR DE TECNOLOGIA DA SAÚDE DE LISBOA

Co-60 source - a study on induction of damages and repair kinetics in a PC3 cell line

Filipe Fernandes Pires

Supervised by Ana Belchior, PhD
Co-Supervised by Margarida Eiras, PhD

MASTER IN RADIATIONS APPLIED TO HEALTH TECHNOLOGIES
- RADIATION THERAPY -

Lisbon, 2018

INSTITUTO POLITÉCNICO DE LISBOA
ESCOLA SUPERIOR DE TECNOLOGIA DA SAÚDE DE LISBOA

Co-60 source - a study on induction of damages and repair kinetics in a PC3 cell line

Filipe Fernandes Pires

Supervised by Ana Belchior, PhD
Co-Supervised by Margarida Eiras, PhD

Dissertation submitted in partial fulfillment of the requirements for the Degree of

MASTER IN RADIATIONS APPLIED TO HEALTH TECHNOLOGIES
- RADIATION THERAPY -

Lisbon, 2018

Declaration

I, Filipe Pires, declare that this thesis, submitted in the fulfillment of the Master's degree at Escola Superior de Tecnologia da Saúde de Lisboa, is wholly my own work unless otherwise referenced or acknowledged appropriately.

Filipe Pires

August 2018

ACKNOWLEDGMENTS

I'm lucky enough to be indebted to a number of people.

First and foremost, I would like to express my deepest gratitude to my supervisor, Professor Ana Belchior, for an amazing opportunity and for a great deal of support and patience throughout the course of the dissertation.

A word of appreciation to Professor Margarida Eiras, as co-supervisor, for the promptness and availability that always characterized her.

I will keep a debt of gratitude to the researchers of GPSR and to the C^2TN in a broader sense, for allowing me a peak in the world of investigation and for keeping the doors of their laboratories and offices always open.

During my time at the center I got acquainted with a couple of fellow students, with whom I had the pleasure to share a well-furnished and organized workspace. I must thank Ana, for being a great teacher and a greater friend and for being such a vast source of wisdom and support. A special mention to João, for being a brave companion in the student's room as well as in the lab. I won't succeed to say "thank you" to Jorge nearly as eloquently as I would like to or as he would be able to, but still, I'd like to emphasize how grateful I am for having him on the adjacent desk. I'd say I didn't know how to repay him, but fortunately I do – take him to David's hole (its tastier than one could assume). My thankfulness to Valerio, for choosing Lisbon as an Erasmus destiny, and for his inconspicuous curiosity toward the meaning of Portuguese vocabulary; if he experienced half of the joy we felt for sharing this year with him, he had a great time. More than personal friends, all of them contributed in some way, either by discussing ideas, helping in research or programming, or reviewing drafts and they prove to be enormously helpful and unselfish with their time.

My sincere gratitude to Alex, Inês and Rita for the moments, adventures and for the laughter in between. I cherish those and I'm longing for new ones, even if I'm forced to endure some appalling music choices.

To my grandmother, "vó", my uncles, Paulo and Di, and my cousins, Miguel and Pedro, I would like to express how deeply lucky I feel for having such unconditional sources of strength and support.

To my mother. Some people claim its actually hard to raise your offspring by means of example. I wouldn't know. It came so natural for her. I'm grateful for that.

CONTENTS

LIST OF TABLES

LIST OF FIGURES

LIST OF ACRONYMS

γ-H2AX	*Phosphorylated H2AX*
53BP1	*Tumor Suppressor p53 Binding Protein 1*
BSA	*Bovine Serum Albumin*
DAPI	*4',6- diamidino-2-phenylindole*
DDR	*DNA Damage Response*
DNA	*DeoxyriboNucleic Acid*
DSB	*Double Strand Break*
FBS	*Fetal Bovine Serum*
FITC	*Fluorescein Isothiocyanate*
IR	*Ionizing Radiation*
IRIF	*Ionizing Radiation-Induced Foci*
H2AX	*Histone family member X*
LET	*Linear Energy Transfer*
LQ	*Linear Quadratic*
PBS	*Phosphate-Buffered Saline*
PCC	*Pearson's Correlation Coefficient*
PE	*Plating Efficiency*
PSA	*Prostate Specific Antigen*
RBE	*Relative Biological Effectiveness*
ROS	*Reactive Oxygen Species*
RPMI	*Roswell Park Memorial Institute medium*
SF	*Survival Fraction*
SSB	*Single Strand Break*
WHO	*World Health Organization*

ABSTRACT

This dissertation was designed to address the study of induction and repair kinetics of Co-60-induced deoxyribonucleic acid (DNA) damages in human prostate tumor cells (PC3 cell line). The analysis aims to investigate the number of complex damage induced in this cell line, to test its repair ability and its influence on cell survival capacity. It is intended that this study contributes to the characterization of the response to a specific radiation source by these malignant prostate tumor cells.

The present work proposes to evaluate the radio-induced effects in the following 24 hours and to observe the integrity of the survival capacity. In the first part, an immunofluorescence assay is performed. Two biomarkers are used, phosphorylated H2AX (γ-H2AX) and tumor suppressor p53 binding protein 1 (53BP1), in order to determine the number of double strand breaks (DSBs) through their correspondence with the foci, identified by antibodies specific to the biomarkers, over several time-points from the first half hour after irradiation up to 24 hours. Subsequently, co-localization between γ-H2AX and 53BP1 is tested using the correlation coefficient provided by CellProfiler. In a second part a clonogenic assay is performed, observing the evolution of the survival fraction with increasing dose.

The results showed that cellular repair after induction of damage allows a decrease of the number of DSBs, but up to 24 hours' post-irradiation there is a level of residual damage present. Between γ-H2AX and 53BP1 there appears to be a partial level of co-localization, with a tendency for decreasing throughout the repair process.

In summary, the work described in this dissertation demonstrates the level of induced damage and repair kinetics of the PC3 cell line, suggesting a dose and time repair dependence.

Keywords: PC3 cell line, low-LET radiation, DSB, γ-H2AX, co-localization

RESUMO

Esta dissertação foi desenhada para abordar o estudo da indução e cinética de reparação de danos na molécula do ácido desoxirribonucleico (DNA), induzidos por Co-60, em células humanas de tumor da próstata (linha celular PC3). A análise pretende investigar o número de danos complexos induzidos nesta linha celular, testar a sua capacidade de reparação e a sua influência na capacidade de sobrevivência. Pretende-se que este estudo contribua para a caracterização da resposta a uma fonte de radiação específica por estas células malignas de tumor de próstata.

O presente trabalho propõe fazer uma avaliação dos efeitos radio-induzidos nas 24 horas seguintes e observar a integridade da capacidade de sobrevivência. Na primeira parte, é realizado um ensaio de imunofluorescência. Dois biomarcadores são utilizados, a H2AX fosforilada (γ-H2AX) e a 53BP1, com o objectivo de determinar o número de duplas quebras de cadeia (DSB) através da sua correspondência com os focos identificados por anticorpos específicos aos biomarcadores, ao longo de diversos pontos no tempo desde a primeira meia hora após irradiação até às 24 horas. Posteriormente, é avaliada a co-localização entre a γ-H2AX e a 53BP1, com recurso ao coeficiente de correlação providenciado pelo CellProfiler. Numa segunda parte é realizado um ensaio clonogénico de sobrevivência, observando a evolução da fracção celular sobrevivente com o aumento da dose.

Os resultados mostraram que a reparação celular após a indução de danos permite diminuir o número de DSB, mas até 24 horas pós-irradiação existe um nível de dano residual presente. Entre os anticorpos, γ-H2AX e a 53BP1, parece haver um nível parcial de co-localização, com uma tendência para este diminuir ao longo do processo de reparação.

Em suma, o trabalho descrito nesta dissertação demonstra o nível de danos induzido e a cinética de reparação da linha celular PC3, sugerindo uma dependência em relação à dose e tempo de reparação.

Palavras-chave: linha celular PC3, radiação de baixo LET, DSB, γ-H2AX, co-localização

1. INTRODUCTION

1.1. MOTIVATION

It was after the discovery of X-rays in 1985, by Wilhelm Conrad Röntgen, that the role of ionizing radiation (IR) began to be appreciated for its potential in diverse applications. The first documented utilization with a clinical application occurs in less than one year after Röntgen manages to see a shadow of his wife's finger bones in a palette. A medical student, Emil Grubbe, used X-rays to treat a 65-year-old woman with a recurrent breast carcinoma, at a factory in Chicago, USA (1).

The World Health Organization (WHO) cancer report places cancer among the major causes of mortality, with a global estimate of 8 million cancer-related deaths annually, with a growing tendency. Prostate cancer presents the second highest incidence rate (31.1 per 100 000), with a mortality rate of 7.8 per 100 000 (2). At present day, the therapeutic application of IR, radiation therapy, is given a protagonist role. Broadly, the therapeutic approaches associated with cancer treatment often include a combination of therapies, of which the more frequent include surgery, chemotherapy, and radiation therapy. More than half of these patients have clinical indication to undergo radiation therapy, with diverse timings and purposes.

The beginning of the story to study the biological effects of IR is marked around the time of Röntgen's discovery and it was driven by the necessity of assessing the effects and potential risks for human health of the uses of IR that were being discovered.

IR has the ability to produce charged particles, through the ionization of atoms, that deposit energy in the surrounding medium. When this "medium" is a cell, ionization events can induce modifications in the constituent biomacromolecules. Resulting damages include losses in function of proteins, deactivation of enzymes, peroxidation of lipids, and ruptures or modifications on the structure of nucleic acids, among others. From all the alterations, deoxyribonucleic acid (DNA) constitutes the critical target because it contains genes/chromosomes that preserve the genetic information, which makes it pivotal for the maintenance of the cellular survival.

Radio-induced DNA changes can vary in frequency and degree of severity and include single strand breaks (SSB), double strand breaks (DSB) or base alterations, among others. DSBs, despite the fact they are not the most common lesions, stand out as

critical. DSBs constitute, by definition, breaks in both strands at a reduced distance from one another, so it's not viable to use the complementary strand as a template. The nonrepair or misrepair of a lesion, presupposes a loss of information during the process of cell division which may lead to genomic instability and cell death (3).

Although the use of IR for therapeutic purposes is relatively recent this sort of damage is not exclusively associated with it. As a bi-product of aerobic respiration, reactive oxygen species (ROS) are produced and are able to induce damages (4). It is estimated that each typical mammalian cell can acquire, on a daily basis, between 1000 to 1,000,000 DNA lesions (4). This induction of damages under normal physiological conditions has forced the cells to naturally keep signalization and repair processes, in order to maintain the genome's integrity (5).

DSB creation triggers a set of events, generically known as the DNA damage response (DDR). The actors involved in DDR can function as predictive biomarkers of cell response. Their study is often divided into either techniques that allow the detection of DNA damages or the ones who allow the observation of underlying repair (6).

One of the first observed modifications is the phosphorylation of serine 139 in the H2 histone family member X *(*H2AX) variant, inducing its phosphorylation in the vicinity of the lesion; the molecule receives the name of phosphorylated H2AX (γ-H2AX). Afterwards, a number of repair proteins will follow. This histone modification is associated to some interesting characteristics, such as the fact that the process is fast, abundant, and presents a good relation with DSB, which makes it a sensitive marker for damage detection (7).

However, although the γ-H2AX measurement may be sensitive, it is not a completely specific marker. It has been suggested that phosphorylation of H2AX can occur by diverse processes, such as DNA replication, apoptosis, or residual damage (7). Furthermore, some authors report findings regarding repair kinetics being cell-dependent processes (8). If the measurement of γ-H2AX cannot be attributed exclusively to DSBs and the foci only measure the response and not the lesions themselves, there is a degree of uncertainty associated to it. One way to increase the strength of the results is to combine the measurement of γ-H2AX with that of other proteins known to be involved in the signaling/repair process of the lesions. Several other proteins were discovered to correlate at the sites of DSBs.

Tumor suppressor p53 binding protein 1 (53BP1), one of many repair factors, was

discovered to co-localize with γ-H2AX, allowing the detection of false positives. The presence of both γ-H2AX and 53BP1 leads to ionizing radiation induced foci (IRIF), providing a spatial indication that signalizes DSBs. The parameters of induction and disappearance of IRIF kinetics reflect the physical characteristics of the IR agent. This way, it is possible to retrieve information about the appearance, repair or nonrepair of DSBs and signalizing DSBs in time.

1.2. STUDIES UNDERTAKEN

The above-mentioned sub-sections aim at describing the studies that were performed in this thesis.

Quantification of DSBs, in PC3 cells, using the γ-H2AX and 53BP1 assays and analysis of DNA repair kinetics

This study aimed at quantifying the induction of DSBs, in PC3 cells, after exposure to Co-60. The main goal consisted of measuring the number of foci, both by the phosphorylation of H2AX and 53BP1. Cells were exposed to 2 and 4 Gy, using a Co-60 source. The induced lesions were analyzed at different time-points. After validating the visualization of induced damage, a study regarding its dependence on two variables was performed: (I) A time dependence study. *For a certain dose, is there a significant difference between a number of time-points?* (II) A dose dependence study. *Is there a significant difference between control cells and cells that were irradiated with different doses?*

Analysis of foci co-localization

Measure the co-localization of the two fluorescence signals, γ-H2AX and 53BP1, studying its dependence on repair time and dose.

Survival curve

A cell survival curve was evaluated through the use of a clonogenic assay. The aim was to understand and relate the induction od DSBs with the maintenance of clonogenic ability.

1.3. CELL LINE

An article published in 1979 report the establishment of the PC3 cell line derived from bone metastases of a grade IV prostate cancer patient, a 62-year-old Caucasian male.

PC3 is a cell line characteristic of prostate small cell carcinoma. It is characterized by the non-expression of androgen receptors or prostate specific antigen (PSA). PC3 cells do not respond to glucocorticoids neither fibroblast growth factors. The cell line exhibits markedly malignant behavior, with high metastatic potential, which stands in contrast with the indolent behavior typically found in the clinical setting. For this reason, PC3 cells tend to be used as a portrayal of the malignant presentation of prostatic tumors (9).

1.4. RADIATION SOURCE

Cobalt-60 is a radioactive isotope of cobalt-59, with an extra neutron and a half-life of 5.26 years. Through a beta- minus process it decays for an excited Ni-60 with an energy of 0.31 MeV and for a stable state emitting two photons, of 1.173 MeV and 1.332 MeV (Figure 1). There are two beta- minus channels; in 99.88 % of the decays follow from Co-60 to the second excited state de Ni-60 with a maximum electron energy of 0.313 MeV. Only 0.1 % of the decays follow from Co-60 to the first excited state of Ni-60 with a maximum electron energy of 1.486 MeV. Co-60 is produced artificially by neutron activation in nuclear reactors (10).

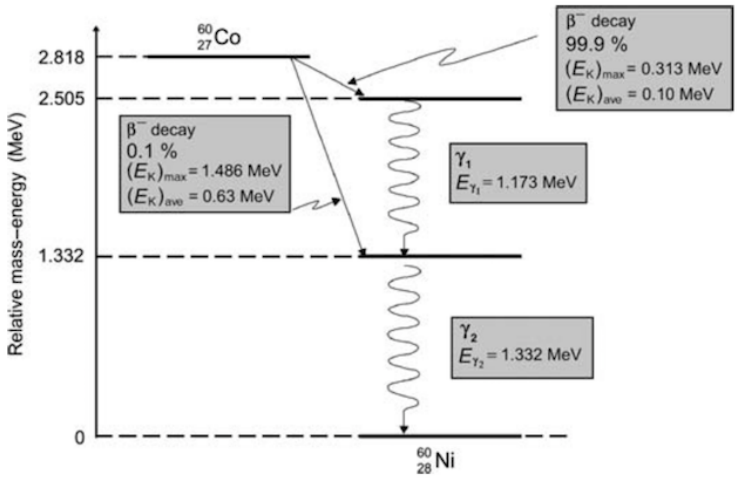

Figure 1: Decay process from Cobalt-60 into Nickel-60. Extracted from (10).

The linear energy transfer (LET) describes the energy transfer from the incident beam to the surrounding medium (11). Historically, much of the use of IR in cancer therapy has been done with low-LET sources, both in brachytherapy, with sources such as iridium-192, cesium-137, and also in external radiotherapy, with electrons and photons. Cobalt-60 sources have a part in both aforementioned approaches. High- LET IR, beams composed of heavy charged particles, have been playing an increasingly more relevant role in the clinic, due to the growing evidence, that describes a greater efficacy in inducing cell damage (11). Regardless, considering of the past and current role of low-LET IR in areas as diverse as radiotherapy or food irradiation, this type of sources possess a robust body of evidence and, therefore, play a major role on the comparison with other types of IR.

For this work the Precisa 22, an experimental equipment (Graviner, Manufacturing Company, Ltd, U.K.) loaded with Co-60 sources was used. It is located at Campus Tecnológico e Nuclear (CTN), Sacavém, Portugal. It should be noted that all irradiations and associated dosimetric procedures were conducted by PhD. Pedro Santos, from the same institution, who kindly granted his time and expertise.

1.5. OBJECTIVES

The main objective of this project was to contribute to the characterization of the PC3 cell line response to radiation. Secondary golds were defined, in order to accomplish this. A study on the induction of DSBs after irradiation was developed. A number of PC3 cells was irradiated with Co-60 sources. Damage repair was measured, using dose and repair time as variables. The co-localization between g-H2AX foci and 53BP1 foci was evaluated, in order to test their relation and its potential usefulness as biomarkers. Finally, an attempt to relate the induced damages with the maintenance of the cell's survival was made, by performing clonogenic assays on the same experimental conditions.

1.6. THESIS OUTLINE

The present dissertation is divided into six chapters. The introduction chapter describes: i) the motivation for the thesis, ii) the studies undertaken, iii) the irradiation source, iv) the cell line used and v) a section-by-section summary.

The second and third chapters intend to provide a theoretical background to the results obtained. The second chapter approaches some key concepts related to the damage induced on the cell line, describing the effects of radiation, the DNA and chromatin, biomarkers of radiation exposure and DNA damage and the actual assays. The third chapter relates to the radiation that leaves the source, the way it interacts with the medium and some basic quantities used to characterize the damage from a physical stand point.

The fourth chapter describes the materials, equipment, and methodologies used. From the maintenance of the cell culture, to the irradiation procedure, the assays, as well as the analysis performed to produce the results.

The fifth chapter presents the results obtained with the different assays, as well as a discussion.

The six and final chapter provides a general conclusion to the work performed during this dissertation and a brief discussion regarding possible future work.

2. BIOLOGICAL EFFECTS OF RADIATION

This chapter begins with an introduction to biological effects and an overview of some theoretical concepts associated with DNA damage. This chapter explains the difference between direct and indirect effects to the DNA, what the DNA is and how it interconnects with the proteins histones to form chromatin. A brief description of some biomarkers of radiation exposure and others types of lesions in the DNA is presented, which will be used in this work. A small theoretical introduction is made in regard to the assays that were performed throughout the dissertation.

2.1. DIRECT AND INDIRECT EFFECT OF RADIATION

IR produces damages by direct and indirect effects, depending on whether the initial events occur in a critical target, such as DNA, or in the cellular environment.

A direct event can be induced directly in DNA, with a subsequent breakdown of molecular bonds. In an indirect way, the damage is induced by free radicals that are mainly originated by the radiolysis of the water, due to its relative abundance in mammalian cells (water can account for 70% or more of its total mass) (12). The energy deposition is done by the ejection of orbital electrons that will induce a cascade of events. The target molecule is converted into an ion pair and then into a free radical. The ejected electrons are free to induce further ionizations. The ionization cycle, the production of free radicals and further release of electrons continues until the photons and particles lose their energy.

X-rays and γ-rays, typical examples of low- LET IR, tend to be associated to indirect effects, whereas particles such as neutrons, alpha particles and other high-LET particles tend to induce mostly direct effects (13).

2.2. DNA AND CHROMATIN

The DNA molecule has two polypeptide chains, consisting of nucleotides (Figure 2). A nucleotide is composed of 3 elements: a sugar, deoxyribose, which is interspersed with a phosphate group forming a backbone, and a base. The base constitutes the only variable element in the composition of a nucleotide and may take one of four forms: adenine, guanine (both purines), cytosine and thymine (two pyrimidines). They follow a rule of complementarity – adenine binds to thymine, whereas citosine binds to guanine; from one strand, it is possible to construct the complementary one. Thus, the double-stranded structure is created, being composed of two sequences that are coiled around each other, forming a double-helix structure (14).

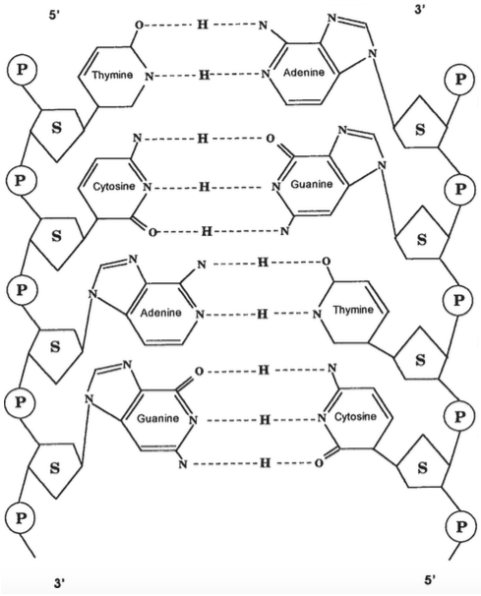

Figure 2: Representation, depicting the DNA double helix, unwound, and the building blocks, the phosphate group (P), the deoxyribose sugar (S), and the bases. Extracted from (14).

Chromatin consists of a combination of DNA and proteins. The DNA is compacted because of its length, although it must remain accessible for biological processes, such as mRNA synthesis, replication, repair of lesions in the strands. The main proteins in the chromatin, histones, are small proteins that facilitate DNA binding. There are five main histones types - H1, H2A, H2B, H3 e H4.

The basic unit of chromatin is called the nucleosome. A nucleosome is composed of 147 nucleotides in length, wrapped in a complex of eight histones, two of each of H2A, H2B, H3, and H4. In order to form a nucleosome, the DNA is first coiled in two H3 and

two H4, followed by the addiction of two dimers of H2A and H2B. The complex is sealed by H1 (14).

Chromatin is present with different levels of compaction. Interphase cells tend to present the chromatin in a more diffuse, unwrapped and active form than the more commonly packaged, typical in division and usually silenced. The level of compaction influences factors such as radiosensitivity and the ability to repair. Uncompressed forms tend to be more sensitive, but also more efficiently repaired than more compacted, less sensitive, forms.

2.3. CELL CYCLE

The cell cycle encompasses the various stages in which a cell goes through since birth, until it is ready to divide and give rise to new cells. It is typically divided into interphase and mitosis.

The Gap 1 (G1) and Gap 2 (G2) are associated to the preparation for the events that characterize the cell cycle: the synthesis phase (S) and the cell division. First, the cell begins to grow to a certain volume, producing all of the cellular components it needs for the next phase, with the exception of the nucleus, in order to duplicate the genetic material. In case the environment is poor in nutrients, the cell remains at this stage until the conditions change. There is an evaluation of the physiological conditions and the environment, which determines the continuation of the course. The cell enters the S phase. An extra copy of the genetic material is created. The G2 phase proceeds to mitosis, and the cell will grow, reorganize. During the mitosis, the cell will divide in two daughter cells, each with the respective sets of genetic material and cellular components. At the end of the process, the cell is first subjected to a nucleokinesis process and then to a cytokinesis process, with cleavage of the nucleus and then the cytoplasm (15).

2.4. BIOMARKERS OF RADIATION EXPOSURE

Damage to the genetic material is strongly correlated with IR-induced cell death, but also with tumor mutations and lesions. The IR can induce various types of damages, from changes in bases, strand breaks, SSB or DSB, among others (Figure 3).

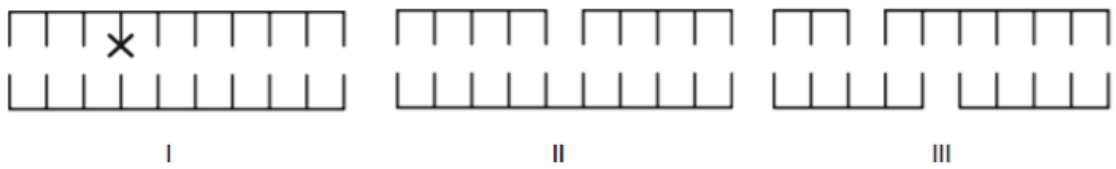

Figure 3: Schematic representation of some DNA damage examples: (I) alteration of bases; (II) SSB; (III) DSB. Adapted from (16).

An altered base can occur by disruption or chemical modification of the bases through ROS, a result of indirect effects.

A SSB corresponds to one or more breaks on a single strand of the DNA backbone. There are two general ways of inducing this type of damage: (i) at the phosphodiester bond level between the phosphate group and deoxyribose; (ii) at the level of the bond between the base and deoxyribose. This type of injury tends to be produced either by ROS or by repairing abasic sites. Taken individually, they are of little biological significance in intact DNA, due to the possibility of repair using the second strand as a template. If the repair is not effective (misrepair), it may result in a mutation. If both strands breaks possess a significant separation, they will be handled separately as individuals SSBs. This type of injury resembles events that occur naturally in the cell. As an example, during the replication phase the double strand must be opened in order to allow access of the replication proteins to the genetic information (12).

DSBs are considered the most relevant type of lesion for the study of radiobiological effects, such as cell death, chromosomal aberrations or carcinogenesis. They consist of two SSBs in opposite strands, at a distance such that base pairing and chromatin structure are insufficient to keep the two joints juxtaposed. DSB can result from two non-time correlated SSBs or two SSBs induced by the same primary event.

A level of complexity can still be added to the repair process if multiple injuries (whether an accumulation of one type of damage or a combination of multiples types) occurs at close distances, in the same strand, or on the opposite one. They form clustered lesions, which, by convention, consists of two or more lesions in a region of 10-20 bp and are usually more difficult to repair because they aren't dealt with in a separate matter (12). IR induces different proportions of lesions, depending on the type of radiation. Due to the higher density of ionizations and excitations along the path, some types of IR will generate a greater proportion of cluster lesions. The proportion of cluster lesions as well as the degree of complexity of each lesion increases with the increase of LET. For a cluster injury to be completely repaired, all components must be

repaired or removed. In addition, several DSBs in proximity increase the likelihood of an incorrect junction of the DNA ends (11,12).

2.5. BIOMARKERS OF DNA LESIONS

2.5.1. γ-H2AX/ 53BP1 FLUORESCENCE ASSAY

DNA damage leads to the modification of the chromatin surrounding the lesions, with the local accumulation of protein complexes, part of a response known as DNA damage response (DRR).

Currently, the quantification of the histone variant X- phosphorylated form H2A, (γ-H2AX foci), represents a well-established method to correlate the DSB formation and the repair kinetics process, serving as a biomarker (17).

The H2A family is constituted by a number of variants, including H2AX. This variant is present in a relative abundance of 2-25 % of the H2A variations, depending on tissue and cell line in analysis (18). Instead of being located in a specific region, it is found in a seemingly dispersed form in histones throughout the DNA. The H2AX protein is unique for its C-terminal tail (COOH). Prior to the stop codon, the tail has a highly-conserved sequence, which includes a serine residue at position 139; this residue is phosphorylated in response to DNA damage.

The γ-H2AX foci formation constitute one of the first responses to DSBs, being capable of extending for up 2 megabase chromatin regions around a lesion in mammalian cells (19, 20).

The phosphorylation process can occur within 1 and 10 minutes after irradiation, and the phosphorylated fraction will increase, peaking at 30 minutes. The fraction of phosphorylated H2AX was found to be proportional to the number of DSBs, with around 0.03% of the phosphorylated H2AX per DSB (21).

After repairing the integrity of the chromatin, γ-H2AX is reversed. If the γ-H2AX signals a destabilization of the chromatin, the signal should be “turned off”, after restoration of the chromatin’s integrity. It has been suggested that this process occurs either by removing the γ-H2AX by histone change or by dephosphorylation by a phosphatase (22). In mammalian cells, the phosphatase 2A (PP2A) appears to be involved in the process of dephosphorylation (22).

Several studies highlight a correlation 1:1 between the number of γ-H2AX foci and the expected number of DSBs induced (21; 23).

Considering the rapid induction and amplification of γ-H2AX, as well as a good agreement with DSBs, this type of study has been considered the gold standard in the detection of this type of damage. It is known empirically that H2AX plays a role in the cellular response to DSBs, since H2AX-deficient cells and mice exhibit a higher sensitivity to IR and have higher levels of spontaneous genomic instability (24, 25).

The literature emphasizes the sensibility of this assay. However, questions have also been raise regarding its specificity, as summarized by Menegakis et al (26).

i. It has been shown that residual γ-H2AX foci may persist after the rejoining process of the initial damage (18);
ii. McManus et al, describes the presence of "small" foci, irrelevant for the DDR and cycle dependent (27);
iii. A dependence on the level of chromatin's condensation (18);
iv. H2AX phosphorylation events may occur without the presence of a DSB lesion (28).

In this context, there is an argument to be made on the validity of using a second biomarker for the fluorescence assay.

TP53 binding protein 1 (53BP1) was first described as a binding partner to the central domain of p53 tumor suppressor protein, it is often mutated in tumors. The 53BP1 gene is located on chromosome15q15-21, encoding a protein consisting of 1972 amino acids, and presents "interaction surfaces" for several proteins involved in DSB repair (29)(30). The first evidence that would play a role in the cellular response to DSBs was the discovery of their migration and accumulation in these breaks following DSB induction treatments. Later, it was observed that, in response to DSB's, 53BP1 moves to lesion sites, where it plays a role in the acute response and DNA repair.

53BP1 foci begin to form 5 minutes after irradiation, at doses as low as 0.5 Gy. The 53BP1 foci number increases linearly over time, peaking at 15-30 minutes after irradiation, and then decreases, to baseline over the next 16 hours (30).

The relevance of this technique was tested in 53BP1 deficient mices; which exhibited immune deficiencies, high sensitivity to IR and genomic instability, with a tendency to develop tumors (31).

The co-localization of 53BP1 foci with other foci known to mark sites of DNA DSBs such as γ-H2AX foci, supports the hypothesis that the 53BP1 foci can closely relate with the number of DSBs (30).

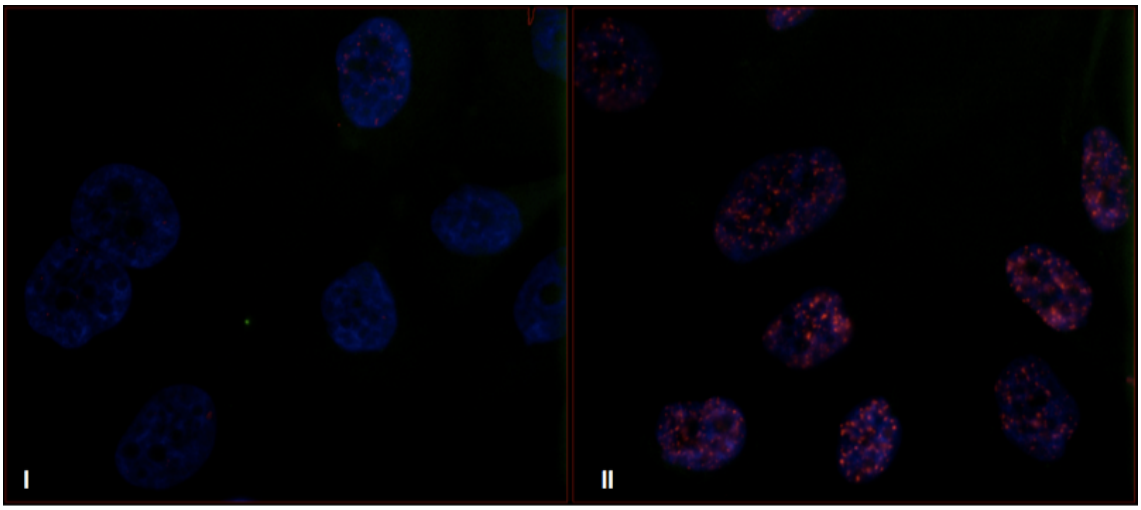

Figure 4: Digital image illustrating IRIF originating from γ-H2AX and 53BP1 in PC3 cells; (I) a control image and (II) a 4 Gy image (both images obtained throughout the course of this work).

To properly quantify DNA damage using immunofluorescence microscopy, cells were treated with two antibodies for each of the foci used in this work (Figure 4). Both protein-primary antibodies and protein-secondary fluorescence antibodies were used. For identification of γ-H2AX foci, a primary antibody (mouse anti γ-H2AX) and FITC-conjugated anti-mouse second antibody were used; whilst for 53BP1 foci, a primary antibody (rabbit anti-53BP1) and Texas Red-conjugated anti-rabbit second antibody were used.

2.5.2. CLONOGENIC ASSAY

The clonogenic assay is a cell survival assay and represents the gold standard *in vitro* method to evaluate the clonogenic potencial of *in vivo* cells (32). Determination of a cell's viability is enabled through the ability to form a colony, which is why is frequently categorized as a viability assay. A colony, by definition, consists of a gathering of at least 50 cells. It represents 5-6 potential cell divisions, depending on the growth rate of a specific cell line (33, 34). The assay's goal is to test the cells for their survival ability – the ability to continue dividing indefinitely, allowing the exclusion of cells with a limited

potential for division, either by inducing sublethal damage or by being in a process of cell differentiation. Survival cells that remain viable after irradiation will form colonies and are subsequently quantified, which allows to withdraw considerations regarding cell survival (Figure 5) (33).

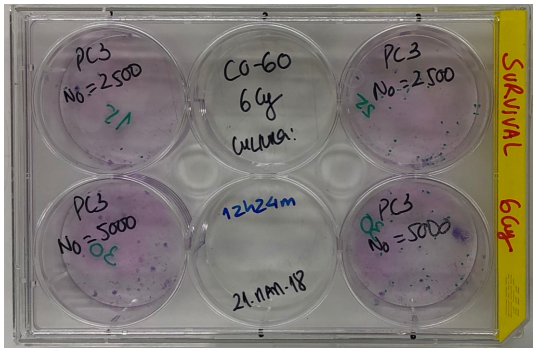

Figure 5: Digital image showing a plate with 4 cultures with colonies derived from a clonogenic survival assay carried out with PC3 cells exposed to a dose of 6 Gy.

The assay allows for an assessment of differences in survival capacity between cells that serve as controls and cells that are exposed to various cytotoxic agents, such as IR or drugs used in chemotherapy. Likewise, it is often applied to monitor the efficacy of several agents by determining their cytotoxic effects at the level of colony formation in different cell lines (34).

3. INTERACTION OF RADIATION WITH MATTER

In this chapter, a brief overview on photons and charged particles interactions with matter is presented, as well as some relevant physical quantities. A description on the basic functioning of an ionization chamber is included.

3.1. INTERACTION OF PHOTONS IN MATTER

In a simplified way, a medium can be seen as a combination of orbital electrons and atomic nuclei, which is composed of protons and neutrons.

When a particle transverses an absorbing material, it interacts with the material's constituent atoms. Photons are indirectly ionizing radiation and so the energy transfer occurs in a two-step process. The incoming photon transfers its kinetic energy to secondary directly ionizing particles, such as electrons. The secondary particles will then deposit their energy through Coulomb interactions (this process will be further developed in the next section).

When a photon transverses a medium, either it interacts or does not interact, maintaining its trajectory. When a photon interacts, multiple processes may occur, depending on factors such as photons energy and chemical composition of the material. When transversing a medium, photon beams mainly experience a loss of intensity, as opposed to the loss of energy verified with directly ionizing particle beams.

An ionization event occurs when the energy transferred by an incident photon is high enough to remove an electron from its orbital. When the transferred energy is lower than the electron's binding energy, the electron is transferred to a more energetic orbital and the atom becomes excited. When the transferred energy is higher than the electron's binding energy, the electron is removed from the atom and the atom becomes ionized (10).

The main physical interactions between photons and matter include the photoelectric effect, Compton scattering, pair production and Rayleigh scattering (Figure 6).

Photoelectric effect. An electron is ejected from one of the orbitals of an atom, induced by the energy absorption of an incident photon. The photon disappears by transferring all its energy, while the orbital electron is ejected with a certain kinetic

energy, leaving the ionized atom. This energy is the result of the difference between the energy of the incident photon and the binding energy of the electron. The electron tends to deposit the energy locally. The vacancy that is open by the ejection of the electron is filled by electrons of outer orbitals, thus inducing one of two competing processes: the emission of characteristic X-rays and of Auger electrons. This process happens when the incident photon's energy is equal or higher than the electron's binding energy (10).

Compton scattering. An incident photon collides with an orbital electron, producing a scattered photon with lower energy, as well as a recoil electron that is ejected from the atom. This phenomenon happens when the energy of the incident photon is much higher than the electron's binding energy (10).

Pair production. A photon with at least 1.022 MeV is converted into an electron and a positron. An electron-positron pair may combine and provoke an annihilation reaction, which, usually results in two photons, each with an energy of 0.51 MeV (10).

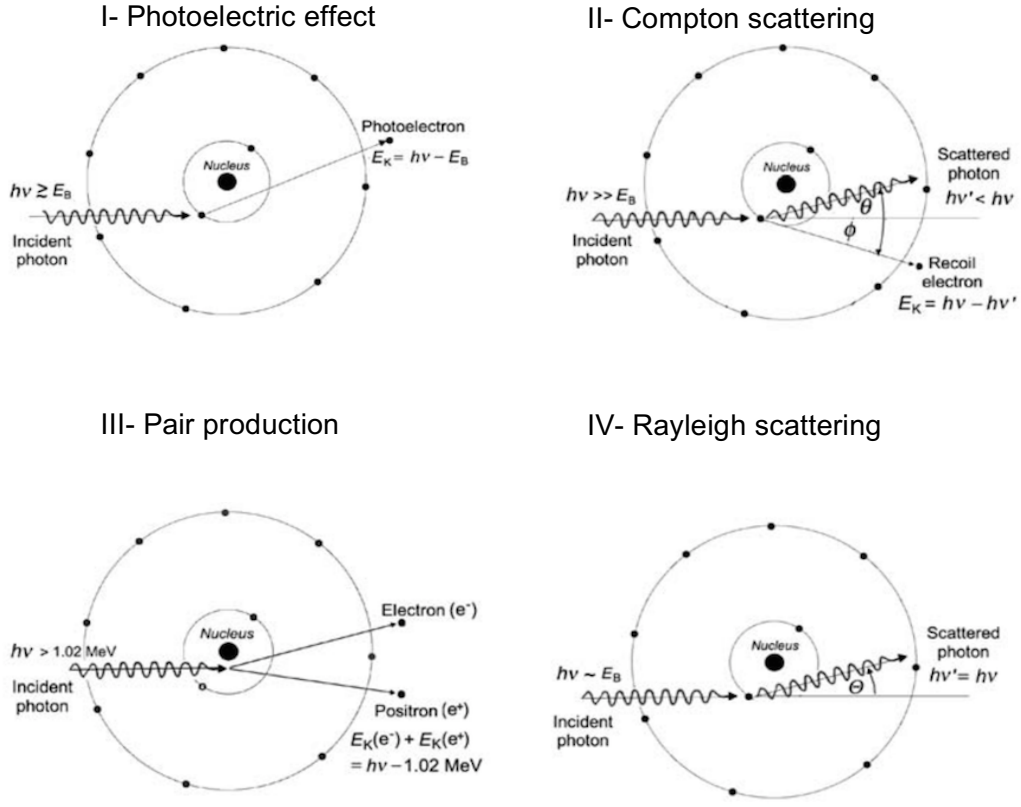

Figure 6: Schematic representation of the main interactions with photons in matter, where (I) corresponds to the photoelectric effect, (II) to the Compton scattering, (III) to the pair production, and (IV) to the Rayleigh scattering. Adapted from (10).

Rayleigh scattering. An incident photon interacts with the absorber atom, being scattered. The scattered photon's energy is very close to the incident photon's energy. An orbital electron in these circumstances accelerates, which causes the atom to emit radiation, to return to a stable state. One of the characteristics of this type of interaction is that the atom does not reach an excited or ionized state. This phenomenon happens when incident photon's energy is approximately equal to the binding energy (10).

3.2. INTERACTIONS OF A CHARGED PARTICLE IN MATTER

Electrons are directly ionizing radiation, thus interacting with matter in diverse ways through Coulomb interactions, being distinguishable through the impact parameter b. It is defined as the smallest distance between the center of the nucleus and the trajectory of the incident particle as it transverses the atom, being measured in relation to the radius of the atom (Figure 7) (10).

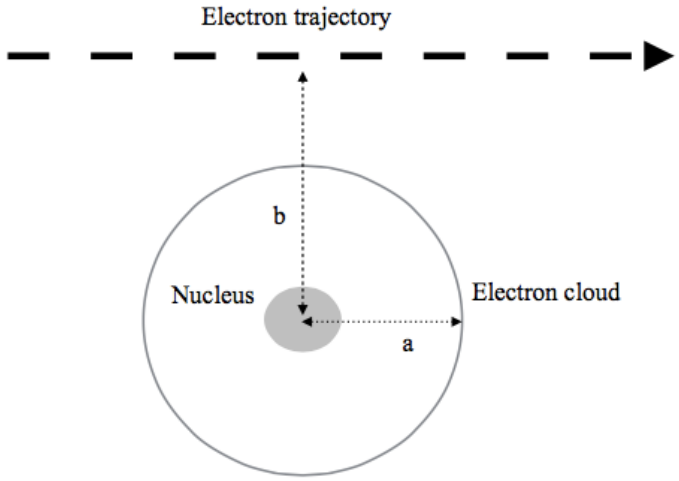

Figure 7: Representation of an electron trajectory in relation to an atom, where a is the radius of the atom and b is the impact parameter. Adapted from (10).

When an incident electron passes at a considerable distance from an atom, that is, the impact parameter b is much higher than the atomic radius ($b >> a$) it is called a soft collision. When the particle transverses the atom, the particle's Coulomb field will interact with the atom's constituent particles, which causes a small amount of energy to be transferred from the incident electron to an orbital electron, which in turn gets excited. Despite the small energy involved in an individual interaction, it becomes relevant due to the high frequency. It is estimate that soft collisions are responsible for

approximately 50 % of a charged particles' energy loss.

When an incident electron passes at such a distance from an atom that the impact parameter b is approximately equal to the radius (b ≈ a) it is called a hard collision. The electron tends to interact mostly with orbital electrons, transferring most of its kinetic energy. If the energy transfer is sufficient to exceed the binding energy of the orbital, the electron is released, thus ionizing the atom. When this electron is able to produce a noticeable track, its named delta ray and it has enough energy to undergo its own Coulomb interactions with other atoms. Although they are less likely, the energy transfer involved is much higher and they account for approximately 50 % of the charged particle's energy loss.

Finally, when the incident electron passes near a nucleus, the impact parameter b is much lower than the atomic radius (b << a) it will experience a Coulomb interaction with the atomic nucleus. An electron may also interact with the orbital electrons of an atom, slowing down due to the repulsive Coulomb interactions and emitting X-rays in the process, known as bremsstrahlung radiation (10).

3.3. PHYSICAL QUANTITIES

3.3.1. ABSORBED DOSE

When a charged particle passes through a medium, it deposits energy along its path. The dose is a measure of the mean energy, E, deposited by IR to matter of mass, m:

$$D = \frac{\Delta E}{\Delta m} \quad \text{Eq. 1}$$

Where

ΔE is the absorbed energy to a mass element Δm and its SI unit is the gray (Gy) (1Gy= 1 $J.kg^{-1)}$ (35).

3.3.2. STOPPING POWER

The loss of energy per path length is defined as stopping power. The total stopping power is the sum of the contributions of two processes: radiative stopping power and collisional stopping power, according to the following expression:

$$-\frac{dE}{dx} = \left(\frac{dE}{dx}\right) col + (\frac{dE}{dx}) rad \quad \text{Eq. 2}$$

The radiation stopping power or nuclear stopping power includes Coulomb interactions with the nucleus. It is related to the emission of photons of bremsstrahlung when an incident particle changes direction along its path. The contribution of this process is particularly relevant in the case of electrons, because they are light charged particles, in a medium with high atomic number.

The collisional stopping power or electronic stopping power results from Coulomb interactions of charged particles with orbital electrons. The contribution of this process is relevant for both light and heavy charged particles. This type of energy loss is associated with the excitation/ ionization of the atoms in the medium (10).

3.3.3. LET

A concept related to stopping power is the linear energy transfer (LET). Constitutes a measure of the average energy locally imparted to the medium by a charged particle of specified energy in traversing a distance dl; it is expressed in keV.μm^{-1}, according to the following equation (35, 36):

$$L_{\Delta} = \frac{dE_{\Delta}}{dl} \quad \text{Eq. 3}$$

in which,

dE_{Δ}, represents the energy transferred to the medium

dl, represents the path length distance

IR is categorized as low-LET or high-LET (Table 1). The low-LET IR usually consists of X-rays. High-LET IR typically includes heavy charged particles and neutrons.

Table 1: Typical LET values of various types of radiation. Usually is considered a value of 10 keV/ μm to separate low from high LET. Extracted from (10).

Low-LET IR	**LET (keV/μm)**	**High-LET IR**	**LET (keV/μm)**
X rays: 250 kVp	2	Electrons: 1 keV	12.3
λ rays: Co-60	0.3	Neutrons	12
X rays: 3 MeV	0.3	Protons: 2 MeV	17
Electrons: 10 keV	2.3	Carbon ions: 100 MeV	160
Electrons: 1 MeV	0.25	Heavy ions	100- 2000

The low-LET and high-LET IR present a different pattern of spatial dose distribution and, consequently, diverse efficiency (Table 2). Low-LET IR deposits the dose relatively homogeneously in the cell's nucleus, presenting a mean spacing between ionizations events in the order of hundreds of nanometers. The high-LET IR tends to deposit a high dose near the particle track and practically none in the area between the tracks, with a higher ionization density.

Table 2: Mean of induced damage in a mammalian cell after administration of 1 Gy, by a low-LET photon beam and by a beam of low-energy α particles (high-LET). Adapted from (37). It should be noted that the induced effects complex with high-LET IR are in greater numbers and a greater part of these damages are not repaired at 8 hours.

Radiation	**Low-LET**	**High-LET**
Tracks in nucleus	1000	2
Ionizations in nucleus	100 000	100 000
Ionizations in DNA	1 500	1 500
DNA SSB	700-1 000	300-600
DNA DSB (initially)	18-60	70
DNA DSB (after 8 h)	6	30
Chromosome aberrations	0.3	2.5

For low-LET IR the ionization events are too spaced relative to the size of a DNA molecule. The result is that a photon can transverse it without depositing energy. For high-LET IR, energy loss events can occur more frequently, as a result, a significant percentage of energy is deposited along the track.

Due to higher ionization density associated with a higher LET value, it is considered to be biologically more effective to have a higher LET value, until around 100 keV/μm. It corresponds to a spatial density of ionization events coincident with the diameter of the DNA strands (about 2 nm).

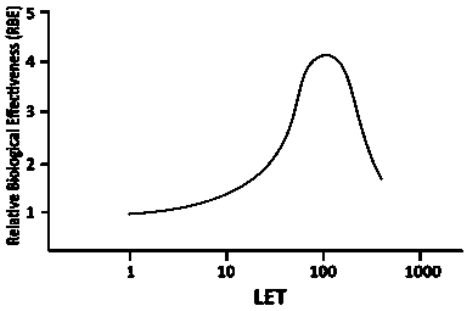

Figure 8: Relation between relative biological effectiveness (RBE) values and linear energy transfer (LET) values. An increase in RBE up to 100-150 keV/μm is observed and a decrease to higher values. Extracted from (37).

To measure the biological efficiency of a certain type of IR, the parameter relative biological effectiveness (RBE) is typically used. RBE is defined as the ratio of a dose of reference radiation (e.g. 250 keV x-rays, RBE=1) to a dose of a given type of radiation that produces an isoeffect. The RBE is dependent to LET, for LET $>$ 10 keV/μm. The RBE value tends to increase with increasing LET values, up to a peak value. After that point, the excessive proximity of events becomes inefficient in regards to the intended target, the DNA molecule (Figure 8) (38).

3.4. DOSIMETRIC SYSTEMS

3.4.1. IONIZATION CHAMBER

The Ionization chamber (IC) is one of the most commonly used dosimeters. ICs can be used for dose determination in reference conditions or to measure relative doses. Although there are a large variety of sizes and shapes, they tend to share a number of common features. IC's usually consist of a gas or liquid- filled cavity, surrounded by a wall made out of a conductive material and a central electrode who serves as a collector. Usually, the sensitive gas present in an ionization chamber will be air. The low-LET IR interacts with the chamber and releases electrons in the chamber wall through photoelectric effect, Compton scattering, and pair production. A percentage of these electrons enter the sensitive volume of the chamber, ionizing the air molecules present, giving rise to positive ions and electrons, of lower energy. These electrons will bond to the oxygen molecules present, forming negative ions. These electrons will bond to the oxygen molecules present in the air, forming negative ions. Therefore, both positive and negative ions will constitute the charged particles that will be collected

(39). The ions pairs, a dose-related, electric current that can be measured using an electrometer (40).

4. MATERIALS AND METHODS

This chapter intends to provide a description of the materials used and the protocols followed throughout the experimental portion and the statistical analysis of the assays. It starts with a description on how the cell culture was maintained, referring the culture medium and supplements. The passage and counting protocol is referred, the latter is also used to test the viability of the cells. This chapter also outlines the irradiation sources, the equipment in which they are inserted in and in which conditions the cultures plates are exposed to them. There's a brief mention to the dosimetry protocol carried out by PhD Pedro Santos. A brief description of the protocols is presented (the followed protocols are detailed in the appendix section). Finally, the methods used to read and analyze the data are outlined.

4.1. CELL CULTURE

4.1.1 Cultivation of Cells

Performing cell cultures is a required step for the study of cell lines. The aim is to create a system that allows for the cells to be maintained, by ensuring them the substances required for their survival and proliferation. Within the scope of this work, a human prostate cancer cell line, PC3, was used. The cell culture was maintained in medium size culture flasks (T-75) (OrFlask, Orange Scientific), in an CO_2 incubator (HeraCell™, Termo Scientific™), with an humidified atmosphere at 37° C, with 5 % CO_2. The preparation of the culture medium for the cell line was carried out according to the manufacturer instructions. The culture medium Roswell Park Memorial Institute medium (RPMI-1640, Sigma Aldrich, St Louis, USA) was supplemented with 10 % fetal bovine serum (FBS) (F7524, Sigma, St Louis, MO, USA), and 1 % of a penicillin streptomycin solution (P4333, Sigma, St Louis, MO, USA). It was kept in storage at 4°C, being heated in a water bath, prior to its utilization. When the cell culture reached approximately 70-80% confluency, a subculture was performed to a new, properly labelled, culture flask, intended to keep the cells in the log phase. This evaluation was made upon visual inspection of the cell density, resorting to an inverted light microscope (Motic AE21). Typically, every 2 days the cells were subcultured. The medium was removed and the adherent cells were washed with PBS. After the PBS

was removed, 2 ml of Trypsin were added and the cells incubated for 2-3 minutes. The cells, rounded, were detached from the flask surface and from one another, after some gentle strokes. This procedure was verified with a microscope. In order to avoid damage, the tryptic activity was inhibited, adding 6 ml of culture medium. Cells were counted (see complete protocol for cell counting in the Annexes section – Protocol Cell Counting) and a fraction was transferred to a new culture flask, already labeled and filled with culture medium. The cell density was re-confirmed at the inverted microscope and at the end the newly prepared culture flask was incubated.

In preparation for the protocols, a specific number of cells was plated onto 6-well culture plates (Z707767 SIGMA, TPP® Merck) 24 hours prior to irradiation, with supplemented culture medium. In the specific case of fluorescence assays, the cells were first placed in cover glass and left to adhere and only after submerged in the culture plates with the culture medium. From the 6-well culture plates, the 2-mid well were not used (see Figure 5, section 2.5.2).

4.1.2. CELL VIABILITY / CELL COUNTING

During the cell counting procedure, it was verified whether the counted cells possessed a blue outline, which translated their viability. The living cells exclude the Trypan Blue (0.4% Sigma Aldrich, St Louis, MO, USA), a negatively charged dye, whilst the non-viable ones, thanks to a compromised cell membrane, allowed the trypan's blue entry. When found, the compromised cells were discarded from the count.

4.2. IRRADIATION PROCEDURE

4.2.1. BRIEF DESCRIPTION OF THE IRRADIATION SOURCE

The irradiations were carried out with the experimental equipment (Precisa 22 (Graviner, Manufacturing Company Ltd, U.K.), loaded with Co-60 sources, located at CTN. The chamber contains four sources of Co-60. The installation consists of a rectangular stainless steel cavity filled with air, with a vaulted upper part. This upper part is arched, with 65 cm height, 50 cm depth, and 20 cm width. The sources are positioned in four stainless steel tubes, located in pairs on the side walls of the chamber, in frontal positions, approximately 30 cm from the floor of the chamber. The movement of the sources inside the tubes, in a length of 50 cm, is controlled

automatically, through an afterloading mechanism, allowing their collection for sample maintenance (41). In order to allow greater homogeneity of dose distribution throughout the samples, the system allows for an automatic rotation of the plate below the samples.

The dose rate used was 1.15-1.18 Gy/min. The sources had an activity of 98 TBq (2657 Ci) at 1st of March and 97 TBq (2628 Ci) at 1st of April. The time required was calculated for the doses used in the present work: 0.5, 1, 2 4, 6 and 10 Gy. The clonogenic assay made use of all the above-mentioned doses plus the control plates. The immunofluorescence assay was evaluated only with 2 and 4 Gy, plus the control plates.

4.2.2. IRRADIATION SETUP

The culture plates were placed on a support (Figure 9), and their position was maintained with adhesive tape.

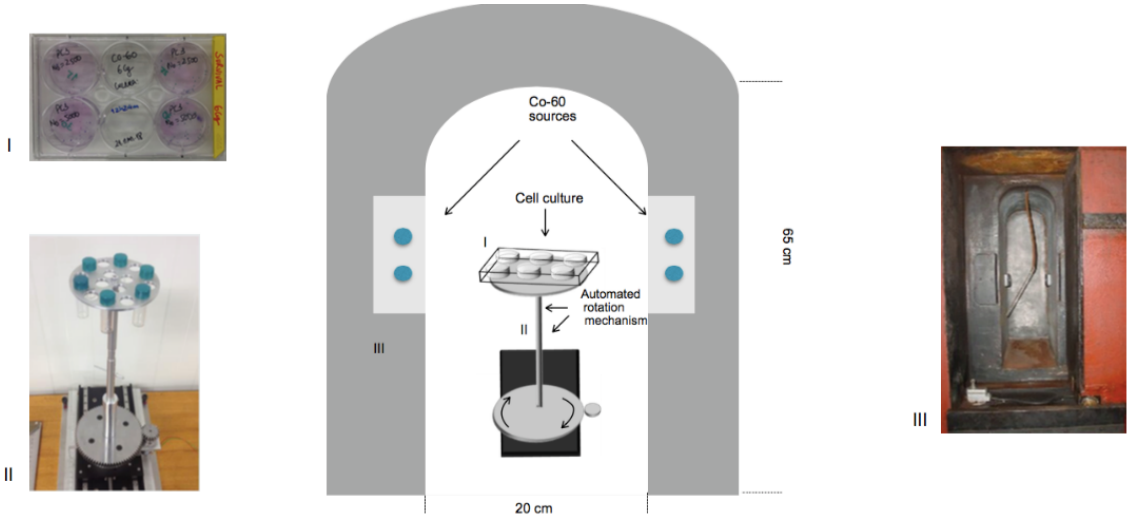

Figure 9: Scheme representing the experimental chamber and the irradiation setup. (I) The culture plate; (II) the rotation mechanism with a base, upon which the culture plates were placed, fixed with adhesive tape, and (III) the interior portion of the chamber.

The path between the irradiation site and the laboratory is covered in less than five minutes. Culture plates were transported in a thermally insulated box at 37°C, maintained with preheated gel packs. Irradiation and all the other steps of the experimental protocols were performed at room temperature, unless otherwise

mentioned.

4.2.3. DOSIMETRY

The calibration of the sources was performed with an IC (Farmer Type Chamber FC65-P, Scanditronix, Wellhofer)(Figure 10). The IC used has a volume of 0.65 cm^3, with a total thickness (wall +build-up cap) of m0.63 g/cm^2 and an electrometer.

Figure 10: Digital image showing the Ionization Chamber (IC) Farmer Type Chamber FC65-P (Scanditronix, Wellhofer).

The dose was measured at 3 points with the IC placed in a rotating support. In rotation, these 3 points covered a circular crown equivalent to the area of the 4 wells used in the 6-well culture plates (also in rotation). The mean value of these 3 registers was adopted. The acquisition was performed on a specific time period, 1 minute, in order to establish a dose rate value (Gy/minute), for the setup used. Using the dose rate value, irradiation times were calculated for each of the intended dose values. Given the uncertainty of the indentation/ advance time of the sources, irradiations were simulated for the intended times and absorbed dose values were checked. Whenever necessary, slight adjustments were made so dose values could be as close as possible to the intended values. The results were reproducible, with very low uncertainties.

4.3. QUANTIFICATION OF THE NUMBER OF DSB LESIONS IN THE DNA

4.3.1. γ-H2AX/ 53BP1 ASSAY

After irradiation, the culture medium was removed and the 200 cells used were washed twice with PBS. A volume of 200 μl per well was used for each step of the process. Irradiated cells were fixed at different times – 30 minutes, 2 hours, 6 hours and 24 hours. Cells were fixed with a 4 % formaldehyde solution for 15 minutes. After being washed twice with PBS, the cells were permeabilised with a solution of Triton X-100

(0.5 %) for 3 minutes.

After being rinsed again with PBS, the cells were incubated with the primary and secondary antibodies. The primary antibodies – mouse anti-γ-H2AX (ab22551, Abcam) and rabbit anti-53BP1 (ab21083, Abcam) were diluted to 1.2 μl/ml and applied to the cells for 45 minutes. The primary antibodies were removed, the cells were washed with with a solution of 1 % BSA. The secondary antibodies – FITC-conjugated goat anti-mouse (ab97239, Abcam) and Texas Red-conjugated goat anti-rabbit (ab6719, Abcam) were diluted to 1.0 μl /ml and applied to the cells for 45 minutes. After, the antibodies were removed and a BSA solution was used to wash the cells. The chromatin was stained with 4',6-diamidino-2-phenylindole dihydrochloride (DAPI, Sigma- Aldrich) and mounted in an anti-fade mounting medium (Vector Laboratories). The full protocol can be found in the annexes section (see protocol in the Annexes – Protocol γ-H2AX/53BP1).

4.3.2. ACQUISITION AND ANALYSIS

Cells were analyzed with an epifluorescent microscope (Zeiss Axioplan 2). The images were acquired using Metafer 4 software (version 2.8.2, MetaSystems™, Altussheim, Germany), which enabled the motorized slide plate to be controlled by the microscope, the filters, and the camera. Depending on the cellular density of each slide, between 30-60 fields were acquired. The images were acquired randomly along the slide and export in RGB format (Figure 11). Subsequently, the images were splitted into 3 individual channels greyscale files in tiff format, using freeware ImageJ (Figure 12) (42). The analysis of the images was performed with freeware CellProfiler 3.0 (43).

4.3.2.1. Foci Counting

A pipeline was created for foci counting, using the provided "ExampleSpeckles" pipeline as a template, obtained through the CellProfiler website (43, 44). For the first 5 images of each subgroup, a manual counting was made, in order to validate and optimize the output provided by the pipeline. Microsoft Excel™ was used for analysing the output provided by CellProfiler and plotting graphs. An outlier analysis was made and the outliers were discarded.

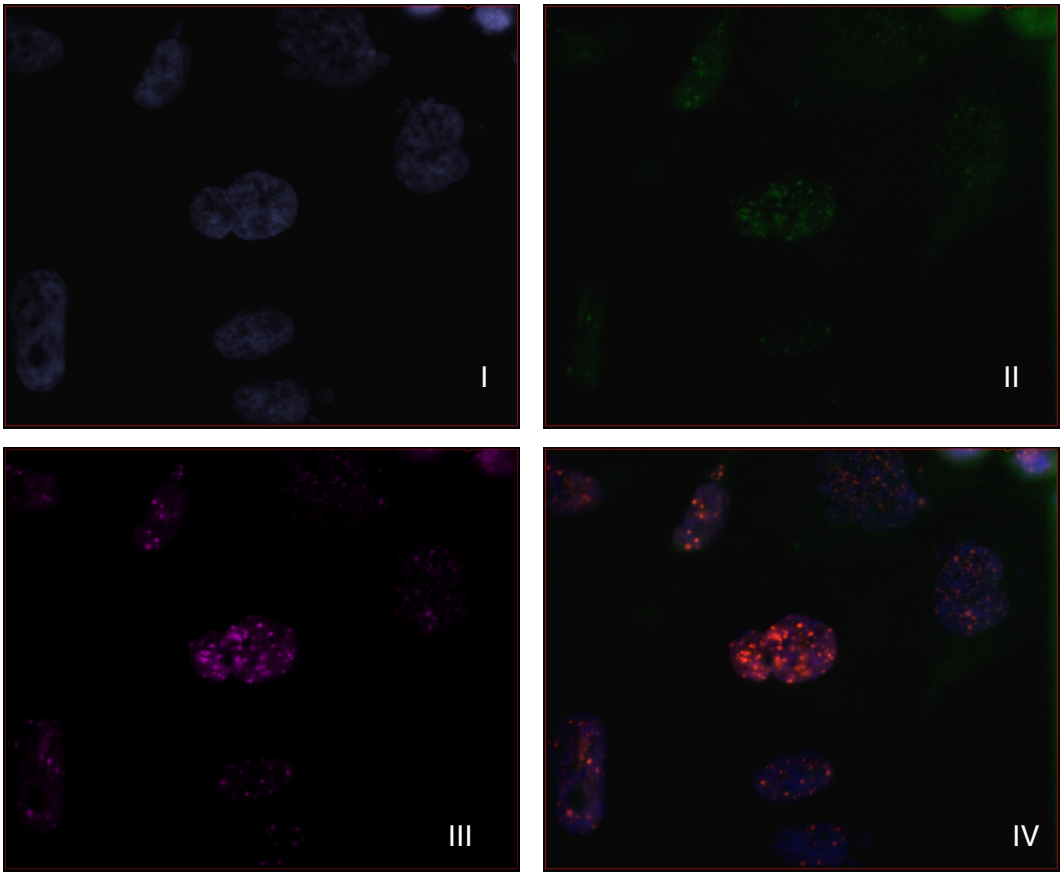

Figure 11: Digital images of (I) nuclei, (II) γ-H2AX, (III) 53BP1, and (IV) the merged image. Represents the ionizing radiation-induced foci (IRIF) and the nucleus of a PC3 cell, 24 hours following irradiation with γ-rays at 4 Gy, obtained in this work.

4.3.2.2. Co-localization

For co-localization between the phosphorylated H2AX and 53BP1, another CellProfiler pipeline was created, using the provided "ExampleColocalization" as a template, obtained through the CellProfiler website. The correlation coefficient, part of the CellProfiler module "Measure Correlation", was also used to analyze the output files.

The correlation coefficient measures the pixel-by-pixel covariance of the pixel's intensity between two images. It subtracts the mean intensity from each pixel's intensity

value, which makes it independent of signal levels and background. This measurement is equivalent to Pearson's correlation coefficient (PCC). The values range from 1 to -1. A value equal to 1 translates two images whose fluorescence intensities are perfectly related, whilst a value of -1 translates two images whose fluorescence intensities are perfectly, but inversely, related to one another (45, 46).

From the correlation coefficient, a mean $\pm$ standard error of the mean (s.e.m.) was calculated. The first and third quartiles were calculated and, from the inter-quartil range, the outliers were removed and the mean $\pm$ s.e.m. was recalculated. The obtained values were plotted. The Microsoft Excel™ was used for analysis of the output provided and plotting graphs. An outlier analysis was made and the outliers were discarded.

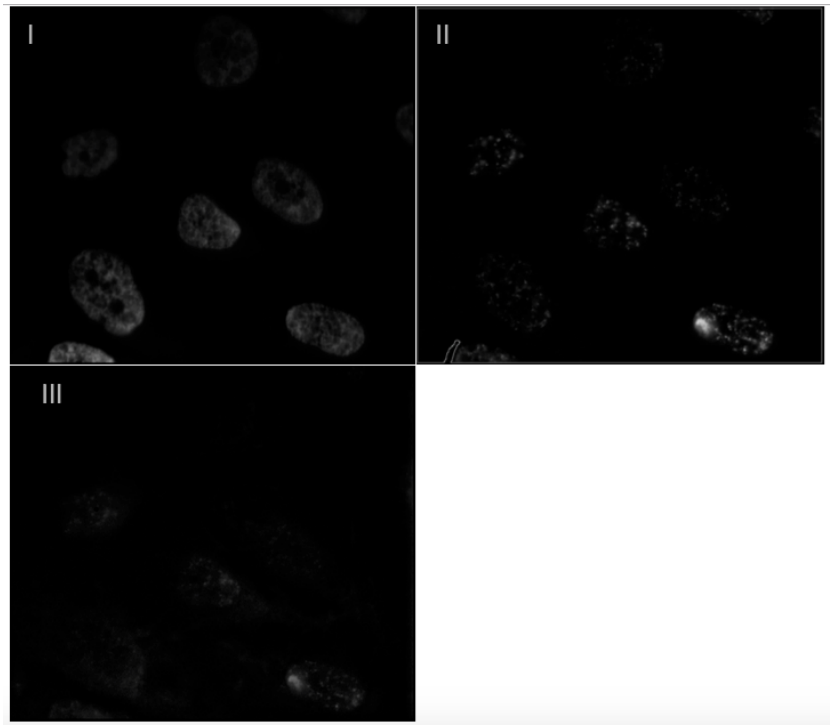

Figure 12: Digital image, exemplifying an output set of images from ImageJ, after being split into separated channels. The exhibited set is from a dose of 2 Gy, acquiring at half an hour after irradiation. (I) Represents the nuclei channel, (II) represents the 53BP1 channel, (III) represents the H2AX channel.

4.4. QUANTIFICATION OF THE SURVIVAL CURVE

A number of diluted cells were placed, into the wells of the culture plates. With the control plates as reference, the cells were seeded for 1-3 weeks, depending on growth rate. The aim was to leave the culture for a time equivalent to at least, 6 cell divisions.

When the colonies from the control plates formed sufficiently large clones (of at least 50 cells), the culture medium was removed and the cells were washed with PBS. The colonies were fixed with a solution of methanol: acetic acid (3:1) and stained with crystal violet (1 %).

The full protocol, based on the work of Franken et al., (33) can be found in the annexes section (see protocol in the Annexes – Protocol Clonogenic Assay).

The number of cells varied, according to the dose. In the control plates, the number varied between 50, 70, and 100 cells. In the 0.5 and 1 Gy plates, the number was either 50 or 100. For the 2 Gy plates, the number of cells was increased to 50, 150, 175, 200 or 250 cells. The 4 Gy plates saw this number vary between 250, 300, and 500 cells. For the 6 Gy, the plates received a number of cells between 2500, 3000, and 5000. Finally, in the 10 Gy plates a number of 25000 or 50000 cells were seeded.

4.4.1. Colony Counting

Colony counting procedure was undertaken with a two-step procedure. First, an operator counted the colonies visible to the naked eye. Afterwards the results were checked/completed with the help of an inverted light microscope (Motic AE21). Colonies of cells were subsequently counted. Platting efficiency (PE) is defined as (33):

$$\mathbf{PE} = \frac{\mathbf{no.of\ colonies\ formed}}{\mathbf{no.of\ cells\ seeded}} \times \mathbf{100} \quad \text{Eq 4}$$

The number of colonies formed after treatment of cells is called surviving fraction (SF). SF is determined based on the control plaques and expressed in terms of PE. This parameter can be calculated according to the following equation (33):

$$\mathbf{SF} = \frac{\boldsymbol{no.}\ \mathbf{of\ colonies\ formed}}{\mathbf{no.of\ cells\ seeded} \times \mathbf{PE}} \quad \text{Eq 5}$$

It is important to calculate the number of colonies formed from the control cells, because it is necessary to calculate the platting efficiency, which will be used to calculate the SF.

4.4.2. ANALYSIS

4.4.2.1 Linear-Quadratic (LQ) model

The linear-quadratic (LQ) model (47) consists in one of the most extensively used models for the quantitative description of IR response. This model describes the survival curve with an equation characterized by two mechanisms of cell killing: non-repairable lesions and repairable lesions (48). The cell survival fraction S with dose D is given by the following equation:

$$\boldsymbol{S} = \exp\left(-\boldsymbol{\alpha D} - \boldsymbol{\beta D^2}\right) \quad \text{Eq 6}$$

Extensive literature has been written on validation of LQ model at low-doses and low-LET IR (49, 50, 51). The survival fraction values are log-transformed and plotted against the dose values experimentally evaluated. An LQ regression analysis was performed, allowing the survival fraction to be described by a second-degree polynomial with two components, α e β (Figure 13)(52). The linear component, α, is associated with the lethal lesions induced by a single radiation track, whilst the β is associated with the lethal lesions induced by two different radiation tracks (51).

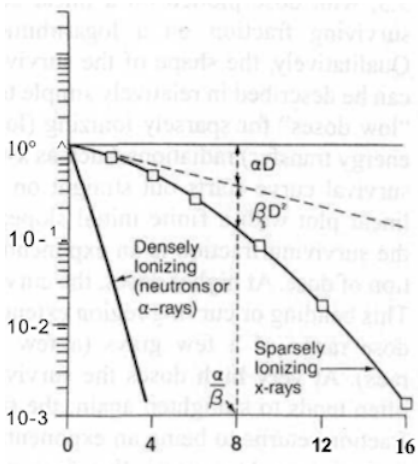

Figure 13: Shape of survival curve. For high-LET IR the dose-response curve consists of a straight line from the origin. For low-LET IR the dose-response curve has an initial linear slope, followed by a shoulder. Extracted from (12).

4.4.2.2 Statistical analysis

The statistical analysis of the clonogenic assay was performed by using a software package, CFAssay for R (R Core Team, R: A Language and Environment for Statistical Computing, 2014). The procedure was adapted from Braselmann et al(32) in order to analyze the survival curve after cell treatment with IR. The results were achieved by

writing and adapting the program to the obtained data, thanks to the expertise of MSc Jorge Borbinha.

The data-points obtained through the clonogenic assay were fitted in the LQ model.

5. RESULTS AND DISCUSSION

This chapter intends to report and discuss the results obtained during the course of this thesis. The measurements from the immunofluorescence assays are presented, divided between the measurements of the number of foci associated with each biomarker, γ-H2AX and 53BP1 and the results of the co-localization between them. These results are analyzed and discussed. The results from the clonogenic assay are also presented and discussed.

5.1. QUANTIFICATION OF THE NUMBER OF DSB LESIONS IN THE DNA

One of the first steps in the cellular response to IR is the phosphorylation of H2AX and 53BP1, being its presence in the nucleus associated with DSBs. The phosphorylated versions can be detected through specific antibodies, leading to the formation of foci. The quantification of these foci allows to test the kinetics of γ-H2AX and 53BP1, thus providing information on the induction of damage and cell repair, making them biomarkers for DSBs (53).

In order to analyze DSBs in the PC3 cell line, the visualized foci were quantified. Their response was assayed in irradiated and non-irradiated cells, over several time-points (30 minutes, 2 hours, 6 hours, and 24 hours). The time-points represent the times the subgroups were given to repair before the process was interrupted. For the 53BP1 foci, the cells were irradiated with a dose of 2 and 4 Gy. For the γ-H2AX only the dose of 2 Gy was evaluated.

The intended goals were to (i) confirm a distinction between a response induced by IR exposure in relation to the basal values encountered in the control groups; (ii) measure the number of DSBs detected by each biomarker at different repair times; (iii) for the 53BP1, measure the number of DSBs detected at different doses.

The mean number of γ-H2AX was measured (Figure 14). For the cells exposed to a single dose of 2 Gy, the maximum value appeared at 30 minutes, with a mean of 22.08 foci/nucleus. The average number of foci decreased with repair time. The biggest decrease occurred from the 6- to the 24-hour mark, from 16.16 foci/nucleus to 9.82 foci/nucleus. The control group presented an average number approximately 5.45 foci/nucleus throughout the different time-points.

The mean number of 53BP1 foci was measured (Figure 15). For the cells exposed to a single dose of 2 Gy, the maximum foci value appeared at 30 minutes, with a mean of 17.53 foci/nucleus. The foci number decreased with repair time. The steepest decrease occurred from 6 to 24 hours, from 13.17 to 7.81 foci/nucleus. The mean foci value at 24 hour-mark remained higher from the value of mean foci in non-irradiated foci, which at 24 hours presents an average number of 4.17 foci/nucleus. For the cells exposed to a single dose of 4 Gy, the maximum foci value also appeared at 30 minutes, with a mean of 28.14 foci/nucleus.

The results obtained allow to draw a pattern, maintained by both biomarkers. A time-dependent trend is noted – as the repair time increases, the mean number of foci per nucleus that is recognizable decreases. Since the foci represent damages recognized by the antibodies, a reduction in foci number reflects a reduction in damage.

The highest difference between mean foci number occurs from 6 to 24 hour, which also represents the highest difference between time-points.

The control culture plates maintained the average number of foci over the time-points, as expected, since they were not exposed to IR. These control groups provided a basal measure of foci needed to assess the difference in damage induced by IR. Moreover, since the plates were exposed to the same procedures, apart from irradiation, they helped excluding any other step in protocol as a cause of damages, like the stress of transport between the irradiation site and the laboratory.

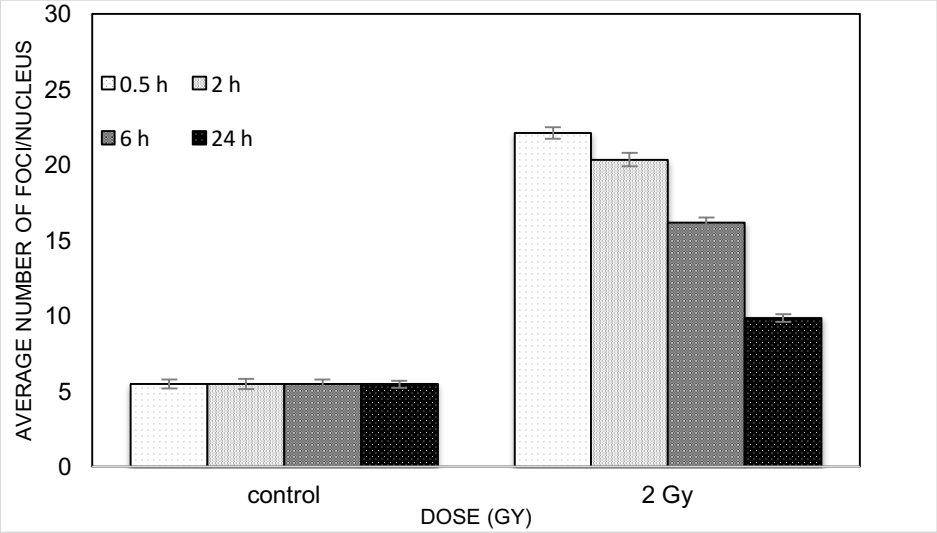

Figure 14: Induction of γ-H2AX foci per nucleus in control cells and in cells irradiated with 2 Gy, after 0.5 (30 minutes), 2, 6, and 24 hours. The error bars associated to each average number represent the standard error of the mean (s.e.m.).

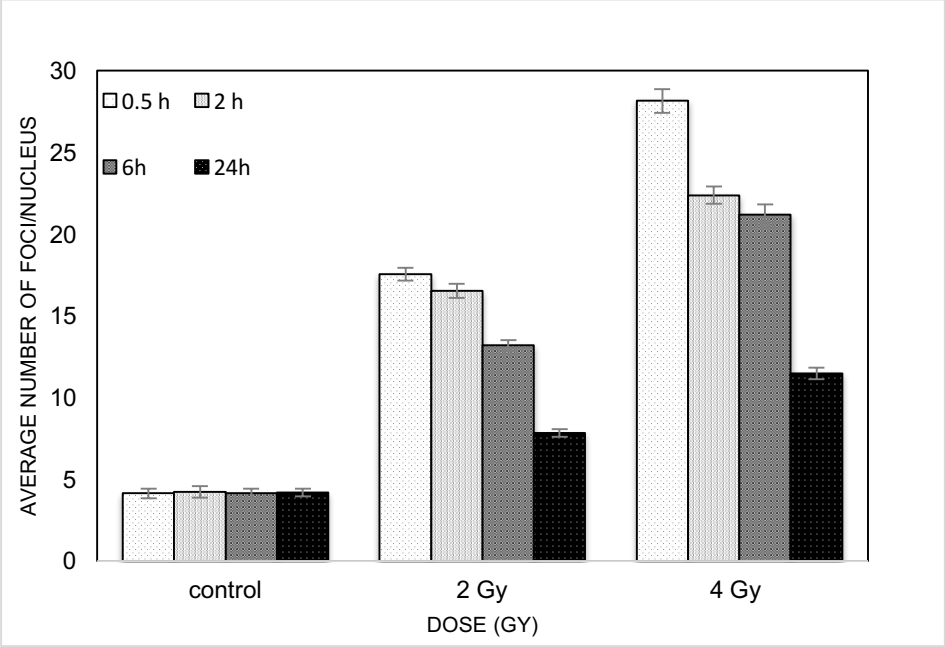

Figure 15: Induction of 53BP1 foci per nucleus in control cells and in cells irradiated with 2 and 4 Gy, after 0.5 (30 minutes), 2, 6, and 24 hours. The error bars associated to each average number represent the standard error of the mean (s.e.m.).

Frequency distribution of the foci number was plotted for both biomarkers, γ-H2AX (Figure 16) and 53BP1 (Figure 17). In order to facilitate visualization of data, the number of foci, represented in the x-axis, was divided in subgroups, rather than presenting the specific frequency for an individual number of foci. In general, an inverse trend is noted in relation to the number of foci per nucleus and repair time – as the repair time increases, the mean number of foci per nucleus decreases.

The frequency distribution for the γ-H2AX and for the 53BP1 foci followed a similar trend: an inverse relation between the number of foci per nucleus and repair time, as observed previously. The dose increment from 2 to 4 Gy, resulted in an increase of frequency of higher number of foci per nucleus, in all time-points evaluated. The control group maintained a stable frequency distribution of foci/nucleus, at the different time-points.

After 24 hours of repair time, the presence of residual foci is still noticeable, since the mean number of foci is higher than the basal number given by the controls. This is in agreement with some of the literature, reporting the presence of some foci after a long period of time after the end of the irradiation, but the significance of these residual foci is not completely clear (54). For that reason, generally, when referring to the relationship described between DSBs and the number of foci, the reference is to the initial number of foci (55).

The γ-H2AX results obtained for the irradiation for 4 Gy were observed to have an intense background. Despite optimization through the pipeline's available modules, CellProfiler was not able to dismiss the background in a consistent manner throughout the tiff files on the diverse time-points. The results were then discarded and time constraints prevented the assay's repetition.

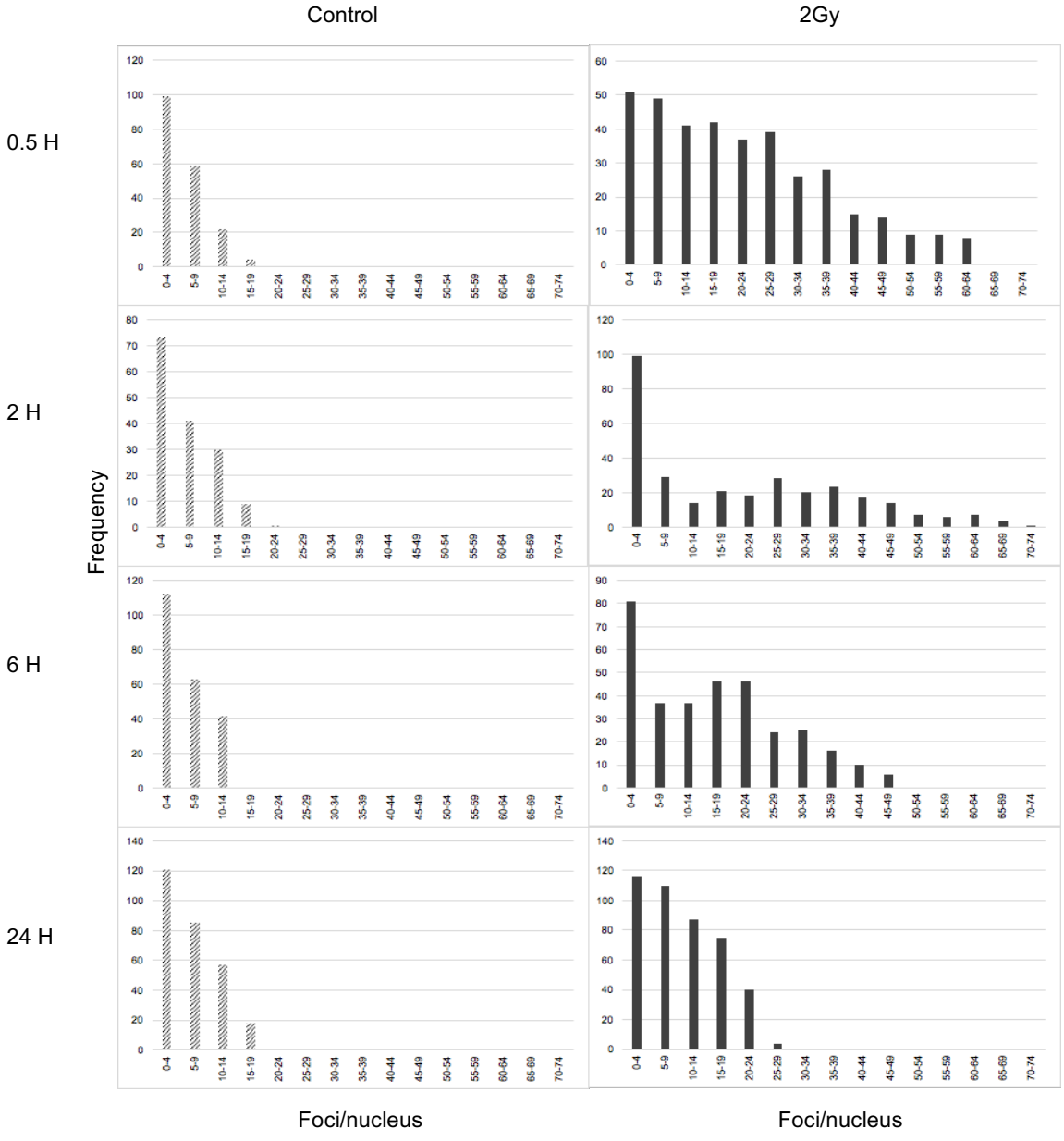

Figure 16: Frequency distribution of the number of γ-H2AX foci per nucleus. The graphs exposed on the left side represent control results, i.e. non-IR-exposed nucleus. The graphs exposed on the right represent results obtained for 2 Gy, i.e. nucleus exposed to a 2 Gy. Several time-points are presented, 0.5 hours, 2 hours, 6 hours, and 24 hours, representing the time intervals between the end of the IR-exposure and the application of the fixation solution. Note that some graphs present different Y-axis values, in order to maintain the overall size.

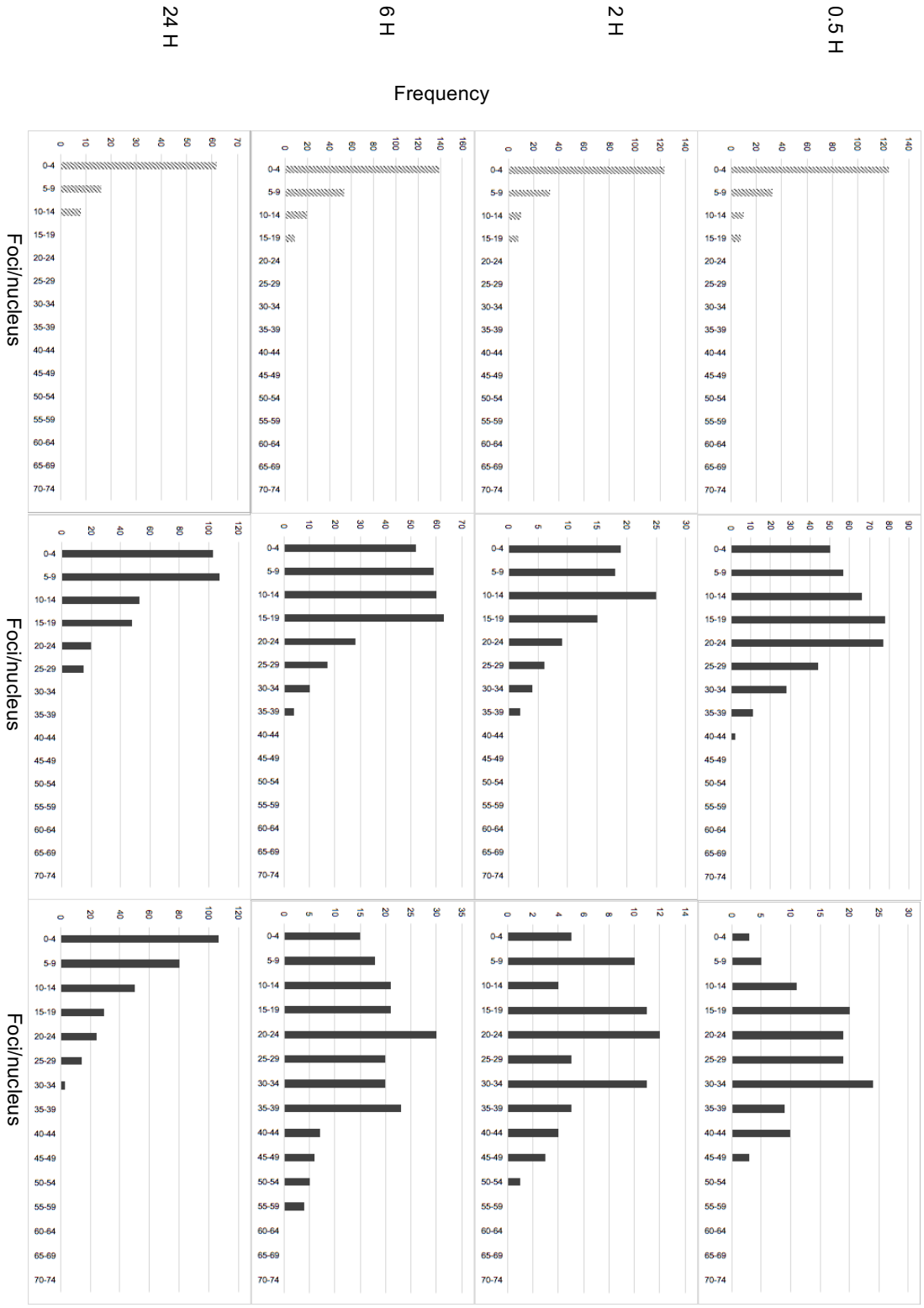

Figure 17: Frequency distribution of the number of 53BP1 foci per nucleus. The graphs represent control results, i.e. non-IR-exposed nucleus, results obtained for 2 Gy, i.e. nucleus exposed to a single dose of 2 Gy and the results obtained for 4 Gy, i.e. nucleus exposed to a single dose of 4 Gy. Several time-points are presented, 0.5 hours, 2 hours, 6 hours, and 24 hours, representing the time intervals between the end of the IR-exposure and the application of the fixation solution. Note that some graphs present different Y-axis values, in order to maintain the overall size.

5.2. ANALYSIS OF FOCI CO-LOCALIZATION

The co-localization of two fluorescence signal distributions was evaluated through the correlation coefficient, calculated by CellProfiler (see section 4.3.2.2). Enables the measurement of the covariance of the pixel's intensity between two images, in each pixel. The experimental results obtained for the control cells and the cells exposed to a 2 Gy dose are shown (Figure 18).

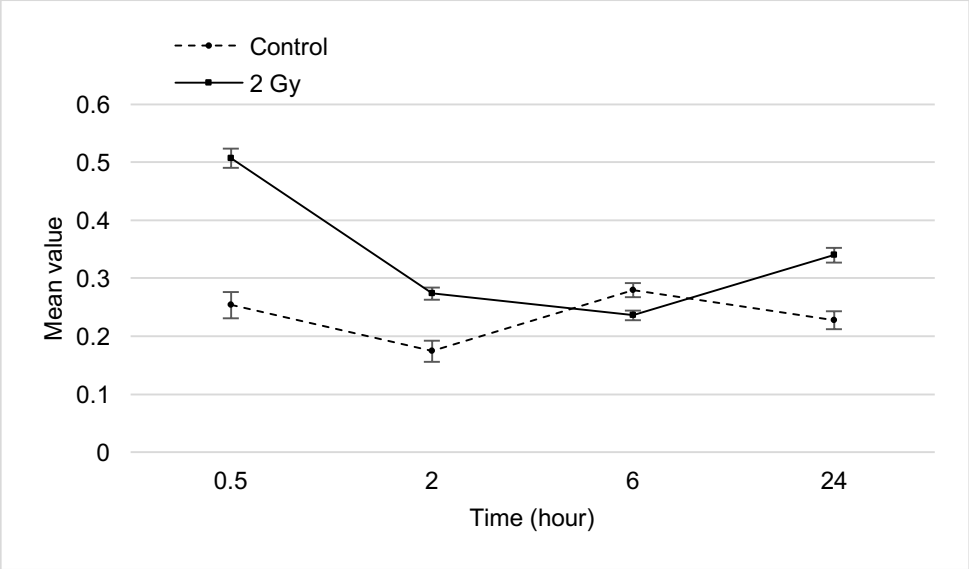

Figure 18: Mean value of colocalization as measured by the correlation coefficient from CellProfiler. The error bars in each mean value represent the s.e.m..

For the 2 Gy curve the maximum value was observed at a 30 minutes' repair time, with a value of approximately 0.51. Between the 30 minutes and 2 hours a large decrease in co-localization was verified, to a value de approximately 0. 27. At 6 hours the value decreased further, to approximately 0.24. A slight increase was also observed toward the 24-hour mark, to a value of 0.34.

The control curve, on the other hand, didn't seem to be characterized by a general trend. There was a decrease from the 30-minute point in relation to a 2 hour repair time, from approximately 0.25 to 0.17. After that, the mean value of co-localization increased to 0.28 for a 6-hour repair time, and decreased again at the 24-hour mark to 0.22. The number of both 53BP1 and γ-H2AX in non-irradiated cells has been found to be significantly different among different cell lines (55).

An overall decreasing tendency is noted as the repair time increases, suggesting the

co-localization to be time-dependent, for the 2 Gy dose points. This is in line with some reports. A tendency is also noted by Marková et al., who refers a lower co-localization at 24 hours in comparison with co-localization at 12 hours, indicating a time-dependence on time post-irradiation. The authors report a dose-dependence as well (55). The evaluation of co-localization at 4 Gy was not possible at this work. Literature still refers the occurrence, in the case of tumor cell lines, of an expression of γ-H2AX in non-irradiated cells (54).

Foci scoring is dependent on the setting threshold criteria for foci size, signal intensity and overall morphology, so as to distinguish "true" foci from antibodies aggregated with diverse targets that are not DSBs. The co-localization of both γ-H2AX and 53BP1 is frequently assumed by literature to be a reflex of the actual DSB number. Still, it is also reported that seemingly spontaneous levels of foci may occur. In addition, it is unclear whether or not they always reflect damages (56). Several authors refer conflicting co-localization levels of γ-H2AX and 53BP1. While a number of authors describe co-localization (57) others do not observe co-localization, or only observe it partially (54, 55).

For the speckles (foci) counting and for co-localization the open source program CellProfiler was used. Poor performance has been reported in situations when images have low signal to noise ratio or sets of images with different levels of background intensity. Some difficulties in optimizing the diverse parameters have also been highlighted (58). For this work both the speckle counting and the co-localization have been used, which are based on pipelines provided as example in the CellProfiler's website. The optimization process was carried out by trial and error, taking a sample of images in several subgroups, divided by biomarker, dose, repair time and image number, and performing a manual counting (for the speckle counting portion of the analysis). The CellProfiler revealed good agreement with 53BP1 after optimization, but not so much so with γ-H2AX, whose high levels of intensity around the nucleus of some image sets prevented a manual counting procedure on those specific images. Among the strategies used to optimize the pipeline, were the threshold for foci size, which was set higher in hopes of removing the background (the same values were used for both biomarkers). We hypothesize that the optimization process might have deleted some of the smaller foci. One alternative would be to repeat the assay and perform manual speckle counting. An article published by Jezkova et al., in 2018, describes this protocol step with two independent experienced evaluators (11). A comparison

between manual and computer-aided foci quantification was made for 53BP1 foci, being reported a difference of no more than 20 % (55). However, nothing is mentioned on the “quality of the images” evaluated.

5.3. QUANTIFICATION OF THE SURVIVAL FRACTION

Clonogenic assays reflect the ability of a cell to survive and continue to proliferate indefinitely, representing the gold standard *in vitro* method to evaluate the clonogenic potential of *in vivo* cells (32).

PC3 cell ability to survive and continue to proliferate was investigated, through a clonogenic assay, using the same experimental conditions used for the immunofluorescence assays. The clonogenic survival of the PC3 cell line was determined in response to a single dose of IR. A colony was defined as having a number greater than 50 cells.

SFs were determined in function of the dose, in Gy. Results are shown in Table 3. The survival (Figure 19), was generated as the result of a fitting process between the experimental data with 7 different single-doses (Table 3), and the LQ model.

Table 3: Values of Survival fraction (SF) obtained through a clonogenic assay. The results are represented as the mean of SF of three independent experiments ± s.e.m.

Dose (Gy)	**Survival Fraction (SF) ± s.e.m.**
0	1
0.5	0.923 ± 0.0696
1	0.651 ± 0.0588
2	0.490 ± 0.0323
4	0.133 ± 0.0114
6	0.042 ± 0.0020
10	0.0002 ± 0.0001

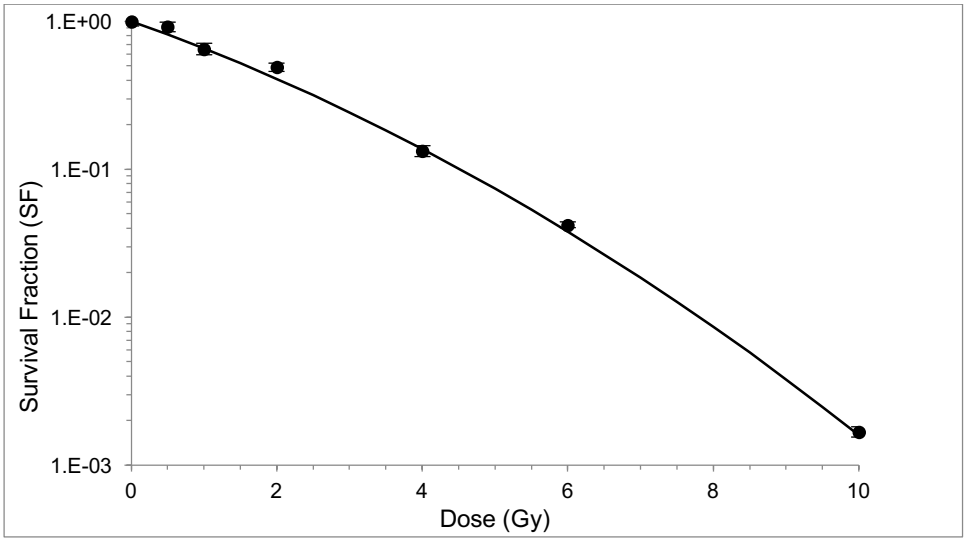

Figure 19: Survival curve for the PC3 cell line obtained from a clonogenic assay. The points represent the mean value of three independent experiences and the s.e.m. is represented by the error bars.

The values of the linear and quadratic parameters of the LQ model were calculated (see section 4.4.2.2.). The equation 7 obtained for the SF of the PC3 cell line was:

$$\boldsymbol{S} = \exp\left(-(-\mathbf{0.39874684})\boldsymbol{D} - (-\mathbf{0.02449586})\boldsymbol{D^2}\right) \quad \text{Eq 7}$$

The PC3 cell line was irradiated with increasingly IR doses. As expected, the irradiation affected PC3 line's survival in a dose-dependent effect, when compared to the non-irradiated cells. Higher IR dose values lead to a lower survival. An initial shoulder was observed, followed by a survival decrease, as dose increased. The obtained α and β values, 0.39874684 and 0.02449586, are in line with those of Van Oorschot et al. This study reports an α value of 0.34 $\pm$ 0.04 and a β value of 0.03 $\pm$ 0.01 , when irradiation is performed with a 250 kev X-ray machine, a dose of 0-8 Gy and a dose rate of approximately 3 Gy/min (59).

6. CONCLUSION

This main objective of this dissertation was to contribute to the characterization of the PC3 cell response to IR. More specific goals were defined, such as: (i) to study of the induction of DSBs soon after irradiation; (ii) to measure, with increasing time, how well the cells repair lesions induced by IR as PC3 are known to be sensitive to radiation; to test cell survival at different doses.

First and foremost, cells were irradiated with different doses, at an experimental chamber loaded with four Co-60 sources. A simple dosimetric study was made, in order to define the amount of time required to deposit the intended doses to the culture plates, where the cells were located.

For the second part, cells were submitted to two different protocols, depending on the cell's intended use. The cells were either let to grow to evaluate the maintenance of the clonogenic potential or to be stripped down of all the components (except for the nucleus) and be placed with antibodies. The antibodies used were designed to identify the biomarkers and emit a fluorescence signal.

The results obtained through the counting of foci by both biomarkers suggest a dose and time dependence regarding the amount of damage. As the cells are given more time to repair, the mean number of foci decreases. Nevertheless, an incomplete repair of damages after 24 hours of irradiation was noted, suggesting a mismatch repair deficiency. The difference between the amount of foci quantified after a repair time of 24 hours and by control groups, suggests the presence of residual DSBs. Residual DSBs are associated with genomic instability and carry a higher risk of IR-induced cell death. This study confirms the radiosensibility of PC3 cells reported by literature.

The literature reports a variety of different data regarding co-localization measurements with heterogeneous results, such as strong co-localizations, partial co-localizations and no co-localization. Due to the poor quality of a portion of the fluorescence images, the pipeline used included several modules, to account for image background heterogeneity. An attempt was made to co-localize the γ-H2AX foci with 53BP1 foci with CellProfiler module "Measure Correlation". Only the images irradiated at 2 Gy presented enough quality to be considered as viable. The correlation coefficient was

used, having obtained a partial correlation on the cells exposed to 2 Gy. In the 2 Gy group, a decreasing tendency was noted in in co-localization as repair times increased. The present co-localization results are consistent with the diverse results found in literature. Still, it is difficult to find a satisfactory explanation for this differences.

Lastly, the survival capacity was tested through a clonogenic survival assay. Calculated α and β values are in agreement with literature and constitute a reference to be compared to upon further studies, either with different IR sources or with difference cell lines.

A major limitation of this study was the need for validation of CellProfiler pipelines, through a manual counting of foci in five randomly selected images. Due to the very high number of samples, this task could not be applied to all of them because it would be laborious and time consuming. Additionally, the poor quality of some images compromised the pipeline's results consistency. If different pipelines were to be developed for different samples, the foci in each image would be counted using different parameters, also jeopardizing result consistency. If time constraints weren't a problem, the course of action would be to repeat the assays, trying to acquire better quality images. We opted for developing a single pipeline, optimizing the modules in order to co-localize counted foci as accurately as possible for all the considered sample images.

We consider the goals pursued during this work to be partially met. We manage to: (i) confirm radiosensibility of the PC3 cell line; (ii) study repair kinetics against basal values; (iii) arrive to partial co-localization values for the group of cells exposed to 2 Gy, considering different repair times; (iv) test survival capacity for a number of dose points. However, bad image quality increases associated with the results obtained in points (i) (ii) and (iii), limiting our confidence in the results and the conclusions that can be drawn from them.

Due to the intrinsic complex cellular response to IR, there is a significant variation associated with radiobiology and biomarker studies. In this sense, studies performed under different conditions provide further insight or underlying cellular response. The work performed during this thesis intends to contribute towards it. The study of cellular response is of uttermost importance to relate radiation damage to normal tissues, as well as to better understand radiation therapeutic effects on tumor cells.

For future studies, some aspects deserve a more in-depth study, such as:

- The contextualization of the results with other cell lines submitted to the same conditions, allowing for a more accurate comparison of repair kinetics.
- The evaluation and comparison of the induction and repair kinetics of DNA damages induced by different types or IR (with different LET values).
- The development of protocols for precise and consistent foci analysis, in the 3D volume of a cell.

PROTOCOL CELL COUNTING

1. Remove the medium from the culture flask
2. Wash 2x with PBS
3. Add a trypsin solution for 2 minutes
4. Check the detachment of the cells with the aid of an inverted light microscope
5. Add culture medium (at least, 3x the volume of trypsin added), homogenizing the resulting solution, pipetting the cell suspension up and down
6. Prepare a 1:1 dilution, adding trypan blue and cell suspension in an Eppendorf tube, homogenizing the resulting solution
7. Transfer 10 μl to an hemocytometer slot
8. Verify the homogeneity using a microscope

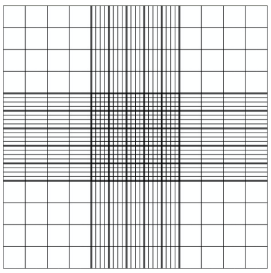

9. Count the number of cells, according to the following equation:

$$\frac{\text{cells}}{\mu\text{l}} = \frac{\text{no. of cells}}{\text{no. of squares}} \times \text{dillution factor} \times \text{camera conversion factor}$$

PROTOCOL γ-H2AX/ 53BP1 ASSAY

CELL CULTURE

1. Add 200 cells to the cover glass (1 per well) and place it on the culture plate after adherence, with a volume of 200 μl of supplemented medium per well, prepared according to the manufacturer instructions. The culture medium RPMI is to be supplemented with 10 % FBS and 1 % of a penicillin-streptomycin solution.
2. Place the culture plates at an CO_2 incubator, with an humidified atmosphere at 37° C, with 5 % CO_2
3. Irradiate the culture plate after 24 h

POST-IRRADIATION

1. According to the damage evaluation timing, remove the culture medium and wash twice with PBS. A solution volume of 200 μl is to be used in every step of the protocol.
2. Add a 4 % formaldehyde fixation solution in PBS for 15 minutes
3. Remove the fixation solution and wash with PBS
4. Add a lysis solution using Triton X-100 (0.5 %) at room temperature for 3 minutes
5. Wash with a solution of PBS
6. Incubate with 1μg/ml primary antibody γ – H2AX/53BP1 for 45 minutes
7. Wash with a 1 % BSA solution
8. Incubate with a FITC/ TxRed secondary antibody at 1 μg/ml for 45 minutes
9. Wash with a 1 % BSA solution
10. Incubate with Hoechst (1 μg/ml) for 5 minutes
11. Wash with a PBS solution and mount with anti-fade

SCORING

1. Cells were analyzed with a fluorescence microscope with a 64x magnification lens
2. The images were randomly obtained and posteriorly exported. The analysis was made using the freeware CellProfiler

PROTOCOL CLONOGENIC ASSAY

CELL CULTURE

1. Add 2500/ 5000 cells to the culture plates, with a volume of 200 μl of supplemented medium per well, prepared according to the manufacturer instructions. The culture medium RPMI is to be supplemented with 10 % FBS and 1 % of a penicillin-streptomycin solution
2. Place the culture plates at an CO_2 incubator, with an humidified atmosphere at 37° C, with 5 % CO_2
3. Irradiate cell in culture after 24 h

POST-IRRADIATION

1. Remove the culture medium and wash with a PBS solution
2. Trypsinize the cells so as to produce a suspension
3. Homogenize and count the cells
4. Dilute the cell suspension with culture medium until reaching the appropriate concentration and place the contents on the culture plates
5. Place the plates in the incubator until the control plates form colonies (time equivalent at least, 6 potential cell divisions)

FIXATION AND STAINING

1. Remove the culture medium and wash thoroughly with PBS
2. Remove the PBS and add a methanol: acetic acid solution (3:1) for 10 minutes
3. Add a staining solution of crystal violet (1%) for 30 minutes
4. Remove the crystal violet solution and rinse with tap water
5. Allow the culture plates to dry at room temperature

COUNTING

1. Count manually the number of colonies

PLATTING EFFICIENCY AND SURVIVING FRACTION

The platting efficiency is determined using the following equation:

$$\mathrm{PE} = \frac{\text{no. of colonies formed}}{\text{no. of cells seeded}} \times 100$$

The number of colonies that form after treatment of the cells, expressed in terms of the PE, is referred to as the surviving fraction, is determined based on the control plates and can be calculated according to equation:

$$\mathrm{SF} = \frac{no.\ \text{of colonies formed}}{\text{no. of cells seeded} \times \mathrm{PE}}$$

REFERENCES

1. Beyzadeoglu M, Ozyigit G, Cuneyt E. Basic Radiation Oncology. Springer - Verlag Berlin Heidelberg; 2010.
2. Stewart BW, Wild CP. World cancer report 2014 [Internet]. World Health Organization. 2014. Available from: http://www.videnza.org/wp-content/uploads/World-Cancer-Report-2014.pdf
3. Su Y, Meador JA, Geard CR, S BA. Analysis of ionizing radiaiton-induced DNA damage and repair in three-dimensional human skin model. Exp Dermatology. 2010;19(8):1–14.
4. White RR, Vijg J. Do DNA Double-Strand Breaks Drive Aging? Mol Cell [Internet]. Elsevier Inc.; 2016;63(5):729–38. Available from: http://dx.doi.org/10.1016/j.molcel.2016.08.004
5. Lomax ME, Folkes LK, O'Neill P. Biological consequences of radiation-induced DNA damage: Relevance to radiotherapy. Clin Oncol [Internet]. Elsevier Ltd; 2013;25(10):578–85. Available from: http://dx.doi.org/10.1016/j.clon.2013.06.007
6. Figueroa-González G, Pérez-Plasencia C. Strategies for the evaluation of DNA damage and repair mechanisms in cancer. Oncol Lett. 2017;13(6):3982–8.
7. Bjergbaek L. DNA Repair Protocols [Internet]. Life Sciences. 2012. 626 p. Available from: http://books.google.com/books?id=Ku2wPAAACAAJ
8. Ochola DO. CORRELATION OF DNA DOUBLE STRAND BREAK REPAIR EFFICIENCY AND SUSCEPTIBILITY TO LUNG TUMOR DEVELOPMENT. 2015.
9. Tai S, Sun Y, Squires JM, Zhang H, Oh WK, Liang CZ, et al. PC3 is a cell line characteristic of prostatic small cell carcinoma. Prostate. 2011;71(15):1668–79.
10. Podgorsak EB. Radiation Physics for Medical Physicists. 2nd ed. Berlin, Germany: Springer - Verlag; 2010.
11. Jezkova L, Zadneprianetc M, Kulikova E, Smirnova E, Bulanova T, Depes D, et al. Particles with similar LET values generate DNA breaks of different complexity and reparability: A high-resolution microscopy analysis of γh2AX/53BP1 foci. Nanoscale [Internet]. Royal Society of Chemistry; 2018;10(3):1162–79. Available

from: http://dx.doi.org/10.1039/c7nr06829h

12. Hall EJ, Phil D. Radiobiology for the Radiologist. 5th ed. [Internet]. Radiology. Lippincott Williams & Wilkins; 2000. Available from: http://pubs.rsna.org/doi/10.1148/radiol.2242022530
13. Gunderson LL, Tepper JE. Clinical Radiation Oncology, 3rd ed [Internet]. Elsevier. 2012. Available from: http://pubs.acs.org/doi/abs/10.1021/ac00291a600
14. Gersen SL, Keagle MB. The Principals of Clinical Cytogenetics - 2nd ed [Internet]. Humana Press. 2010. Available from: http://www.ncbi.nlm.nih.gov/pubmed/22994157
15. Azevedo C, Sunkel C. Biologia Celular e Molecular. Lidel; 2012.
16. Sonntag C Von. Free-Radical-Induced DNA Damage and Its Repair: A Chemical Perspective. Springer; 2006.
17. Ivashkevich A, Redon CE, Nakamura AJ, Martin RF, Martin OA. USE OF THE γ-H2AX ASSAY TO MONITOR DNA DAMAGE AND REPAIR IN TRANSLATIONAL CANCER RESEARCH. Cancer Lett. 2013;327:123–33.
18. Kinner A, Wu W, Staudt C, Iliakis G. Gamma-H2AX in recognition and signaling of DNA double-strand breaks in the context of chromatin. Nucleic Acids Res. 2008;36(17):5678–94.
19. Bönisch C, Hake SB. Histone H2A variants in nucleosomes and chromatin: More or less stable? Nucleic Acids Res. 2012;40(21):10719–41.
20. Paull TT, Rogakou EP, Yamazaki V, Kirchgessner CU, Gellert M, Bonner WM. A critical role for histone H2AX in recruitment of repair factors to nuclear foci after DNA damage. Curr Biol. 2000;10(15):886–95.
21. Pilch DR, Sedelnikova OA, Redon C, Celeste A, Nussenzweig A, Bonner WM. Characteristics of γ-H2AX foci at DNA double-strand breaks sites. Biochem Cell Biol [Internet]. 2003;81(3):123–9. Available from: http://www.nrcresearchpress.com/doi/abs/10.1139/o03-042
22. Chowdhury D, Keogh MC, Ishii H, Peterson CL, Buratowski S, Lieberman J. γ-H2AX dephosphorylation by protein phosphatase 2A facilitates DNA double-strand break repair. Mol Cell. 2005;20(5):801–9.
23. Mariotti LG, Pirovano G, Savage KI, Ghita M, Ottolenghi A, Prise KM, et al. Use of the γ-H2AX assay to investigate DNA repair dynamics following multiple radiation exposures. PLoS One. 2013;8(11):1–12.
24. Celeste A. Genomic Instability in Mice Lacking Histone H2AX. Science (80-)

[Internet]. 2002 May 3;296(5569):922–7. Available from: http://www.sciencemag.org/cgi/doi/10.1126/science.1069398

25. Celeste A, Difilippantonio S, Difilippantonio MJ, Capetillo OF-. H2AX Haploinsufficiency Modifies Genomic Stability and Tumor Susceptibility. Cell [Internet]. 2003;114(3):371–83. Available from: http://www.ncbi.nlm.nih.gov/pubmed/28299348
26. Menegakis A, Yaromina A, Eicheler W, Drfler A, Beuthien-Baumann B, Thames HD, et al. Prediction of clonogenic cell survival curves based on the number of residual DNA double strand breaks measured by γh2AX staining. Int J Radiat Biol. 2009;85(11):1032–41.
27. Bonner WM, Redon CE, Dickey JS, Nakamura AJ, Olga A, Solier S, et al. γH2AX and cancer. Nat Rev Cancer. 2008;8(12):957–67.
28. Soutoglou E, Misteli T. Activation of the Cellular DNA Damage Response in the Absence of DNA Lesions. Science (80-) [Internet]. 2008 Jun 13;320(5882):1507–10. Available from: http://www.sciencemag.org/cgi/doi/10.1126/science.1159051
29. Zimmermann M, de Lange T. 53BP1: pro choice in DNA repair. Trends Cell Biol [Internet]. 2014 Feb;24(2):108–17. Available from: http://linkinghub.elsevier.com/retrieve/pii/S0962892413001554
30. Mochan TA, Venere M, DiTullio RA, Halazonetis TD. 53BP1, an activator of ATM in response to DNA damage. DNA Repair (Amst). 2004;3(8–9):945–52.
31. Ward IM, Minn K, Deursen J Van, Chen J. p53 Binding Protein 53BP1 Is Required for DNA Damage Responses and Tumor Suppression in Mice These include : p53 Binding Protein 53BP1 Is Required for DNA Damage Responses and Tumor Suppression in Mice. 2003;23(7):2556–63.
32. Braselmann H, Michna A, Heß J, Unger K. CFAssay: Statistical analysis of the colony formation assay. Radiat Oncol [Internet]. Radiation Oncology; 2015;10(1):1–6. Available from: http://dx.doi.org/10.1186/s13014-015-0529-y
33. Franken NAP, Rodermond HM, Stap J, Haveman J, van Bree C. Clonogenic assay of cells in vitro. Nat Protoc. 2006;1(5):2315–9.
34. Rafehi H, Orlowski C, Georgiadis GT, Ververis K, El-Osta A, Karagiannis TC. Clonogenic Assay: Adherent Cells. J Vis Exp [Internet]. 2011;(49):15–7. Available from: http://www.jove.com/index/Details.stp?ID=2573
35. Seltzer SM, Bartlett DT, Burns DT, Dietze G, Menzel H-G, Paretzke HG, et al. ICRU Report 85: Fundamental Quantities and Units for Ionizing Radiation. J

ICRU. 2011;11(1):1–35.

36. 3. Definition and Concepts of LET [Internet]. Journal of the International Commission on Radiation Units and Measurements. 1970 Jun. Available from: https://academic.oup.com/jicru/article/2924148/3.
37. Okayasu R. Repair of DNA damage induced by accelerated heavy ions-A mini review. Int J Cancer. 2012;130(5):991–1000.
38. Paganetti H. Proton Therapy Physics [Internet]. Health Physics. 2012. 690 p. Available from: http://www.lavoisier.fr/livre/notice.asp?id=RK2W6SA2XKKOWQ
39. Togno M. A novel ion chamber technology for quality assurance in external beam radiotherapy. TECHNISCHE UNIVERSITÄT MÜNCHEN; 2017.
40. Podgorsak EB. Radiation Oncology Physics: A Handbook for Teachers and Students. International Atomic Energy Agency. 2005.
41. Belchior A, Botelho ML, Vaz P. Monte Carlo simulations and dosimetric studies of an irradiation facility. Nucl Instruments Methods Phys Res Sect A Accel Spectrometers, Detect Assoc Equip. 2007;580(1 SPEC. ISS.):70–2.
42. ImageJ. Available from: https://imagej.net/Welcome
43. Carpenter AE, Jones TR, Lamprecht MR, Clarke C, Kang I, Friman O, et al. CellProfiler: image analysis software for identifying and quantifying cell phenotypes. Genome Biol [Internet]. 2006;7(10). Available from: http://genomebiology.biomedcentral.com/articles/10.1186/gb-2006-7-10-r100
44. CellProfiler Project.
45. Dunn KW, Kamocka MM, McDonald JH. A practical guide to evaluating colocalization in biological microscopy. Am J Physiol Physiol [Internet]. 2011 Apr;300(4):C723–42. Available from: http://www.physiology.org/doi/10.1152/ajpcell.00462.2010
46. Adler J, Parmryd I. Quantifying colocalization by correlation: The pearson correlation coefficient is superior to the Mander's overlap coefficient. Cytom Part A. 2010;77(8):733–42.
47. Chadwick K, Leenhouts H. The molecular target theory of cell survival and its application in radiobiology. European Atomic Energy Community. 1973.
48. Garcia L, Leblanc J, Wilkins D, Raaphorst G. Fitting the linear-quadratic model to detailed data set for different dose ranges. Phys Med Biol [Internet]. 2006 Jul;51:2813–23. Available from: http://doi.wiley.com/10.1118/1.2031029
49. Kirkpatrick JP, Meyer JJ, Marks LB. The Linear-Quadratic Model Is Inappropriate to Model High Dose per Fraction Effects in Radiosurgery. Semin Radiat Oncol.

2008;18(4):240–3.

50. Zhao L, Mi D, Hu B, Sun Y. A generalized target theory and its applications. Sci Rep [Internet]. Nature Publishing Group; 2015;5:1–11. Available from: http://dx.doi.org/10.1038/srep14568
51. Chris Wang CK, Zhang X. A nanodosimetry-based linear-quadratic model of cell survival for mixed-LET radiations. Phys Med Biol. 2006;51(23):6087–98.
52. Unkel S, Belka C, Lauber K. On the analysis of clonogenic survival data: Statistical alternatives to the linear-quadratic model. Radiat Oncol [Internet]. Radiation Oncology; 2016;11(1):1–11. Available from: http://dx.doi.org/10.1186/s13014-016-0584-z
53. Redon CE, Dickey JS, Bonner WM, Sedelnikova O a. Gamma-H2AX as a biomarker of DNA damage induced by ionizing radiation in human peripheral blood lymphocytes and artificial skin. Adv Sp Res. 2009;43(8):1171–8.
54. Yoshikawa T, Kashino G, Ono K, Watanabe M. Phosphorylated H2AX foci in tumor cells have no correlation with their radiation sensitivities. J Radiat Res. 2009;50(2):151–60.
55. Marková E, Schultz N, Belyaev IY. Kinetics and dose-response of residual 53BP1/γ-H2AX foci: Co-localization, relationship with DSB repair and clonogenic survival. Int J Radiat Biol. 2007;83(5):319–29.
56. Barnard S, Bouffler S, Rothkamm K. The shape of the radiation dose response for DNA double-strand break induction and repair. Genome Integr [Internet]. Genome Integrity; 2013;4(1):1. Available from: Genome Integrity
57. Schultz LB, Chehab NH, Malikzay A, Halazonetis TD. p53 Binding Protein 1 (53BP1) Is an Early Participant in the Cellular Response to DNA Double-Strand Breaks. J Cell Biol [Internet]. 2000;151(7):1381–90. Available from: http://www.jcb.org/cgi/content/full/151/7/1381
58. Lapytsko A, Kollarovic G, Ivanova L, Studencka M, Schaber J. FoCo: A simple and robust quantification algorithm of nuclear foci. BMC Bioinformatics [Internet]. BMC Bioinformatics; 2015;16(1):17–9. Available from: http://dx.doi.org/10.1186/s12859-015-0816-5
59. Van Oorschot B, Hovingh SE, Rodermond H, Güçlü A, Losekoot N, Geldof AA, et al. Decay of γ-H2AX foci correlates with potentially lethal damage repair in prostate cancer cells. Oncol Rep. 2013;29(6):2175–80.